CH 4 -clathrates in Clay Minerals and Sulfate Brines: Application to Gale Crater on Mars

Victoria Muñoz-Iglesias, Elodie Gloesener, Carolina Gil-Lozano, Mathieu Choukroun, Olga Prieto-Ballesteros, Oscar Ercilla Herrero, Maite Fernández Sampedro, Valentín García Baonza, Gabriel Tobie

The Planetary Science Journal, 7:106 (25pp), 2026 May https://doi.org/10.3847/PSJ/ae63c1

CH_4-clathrates in Clay Minerals and Sulfate Brines: Application to Gale Crater on Mars

Victoria Muñoz-Iglesias[1,2], Elodie Gloesener[3], Carolina Gil-Lozano[4], Mathieu Choukroun[5], Olga Prieto-Ballesteros[1], Oscar Ercilla Herrero[1], Maite Fernández Sampedro[1], Valentín García Baonza[6], and Gabriel Tobie[2]
[1] Centro de Astrobiología (CAB), CSIC-INTA, Carretera de Ajalvir km 4, 28850 Torrejón de Ardoz, Madrid, Spain; victoria.munoz.iglesias@gmail.com
[2] Nantes Université, Univ Angers, Le Mans Université, CNRS, Laboratoire de Planétologie et Géosciences, LPG, UMR 6112, France
[3] Univ. Lille, CNRS, UMR 8523—PhLAM—Physique des Lasers Atomes et Molécules, F-59000 Lille, France
[4] Centro de Investigación Mariñas, XM1, Universidade de Vigo, Vigo, Spain
[5] Jet Propulsion Laboratory, California Institute of Technology, Pasadena, CA, USA
[6] Malta-Consolider Team and Departamento de Química Física, Facultad de Ciencias Químicas, Universidad Complutense de Madrid, Plz. Ciencias 2, E-28040 Madrid, Spain
Received 2026 January 26; revised 2026 April 20; accepted 2026 April 21; published 2026 May 13

Abstract

The Curiosity rover uncovered new evidences of fluvial-deltaic deposits at the Gale crater, suggesting the existence of a long-lasting lake in the past. Additional observation of methane (CH_4) emanations has led to the idea that the past water-rich environment was also conducive to the stabilization of CH_4-clathrates in the subsurface. If we consider that one of the possible sources of CH_4 can come from subsurface clathrates, it is crucial to determine whether other secondary minerals coexisting in the underground, such as clay minerals and/or salts, affect their stability. Both clay minerals and salts may affect clathrate thermodynamics and kinetics, as they can decrease gas availability through gas adsorption on clay surfaces or salting-out effects. In this work, we experimentally studied the kinetics of formation and dissociation of CH_4-clathrates in the presence of $MgSO_4$ brines and two types of clay minerals, i.e., one montmorillonite (2:1 type), and kaolinite (1:1 type), by differential scanning calorimetry. The results showed that the presence of both sulfates and clay minerals at high concentrations can favor the induction time of clathrate formation, but reduce the final amount of clathrates. Both the salting out effect caused by the salts and the water being strongly bonded to the clay surfaces are the main factors that prevent clathrate growth. These results have important implications for evaluating clathrates as a potential source for the CH_4 detections in Gale, since the experiments demonstrate the inhibition of clathrate crystallization within mineral associations found in the crater.

Unified Astronomy Thesaurus concepts: Planetary dynamics (2173)

1. Introduction

Identifying the methane (CH_4) origin and fate in the Martian atmosphere remains a major challenge in our understanding of atmospheric physics and chemistry on Mars, as well as planet habitability. Detections of trace amounts of methane on Mars have been reported by four independent groups (V. Formisano et al. 2004; V. A. Krasnopolsky et al. 2004; M. J. Mumma et al. 2009; C. R. Webster et al. 2015). However, the presence of this gas in the Martian atmosphere is still debated (K. Zahnle et al. 2011; G. L. Villanueva et al. 2013; K. Zahnle 2015; C. R. Webster et al. 2018). Given the relatively short lifetime of CH_4 predicted by photochemical models (F. Lefèvre & F. Forget 2009), the observed CH_4 seasonal variability implies the presence of localized active sources and/or sinks, which currently remain unknown. In situ measurements of atmospheric CH_4 performed by the Curiosity rover at the Gale crater (4.5°S, 137.4°E) revealed strong seasonal variations in CH_4 background levels, which reach a maximum at the end of the northern summer (up to ~0.65 ppbv), as well as transient spikes (up to ~20 ppbv; C. R. Webster et al. 2018, 2021). Conversely, recent Trace Gas Orbiter (TGO) observations (O. Korablev et al. 2019; E. W. Knutsen et al. 2021) did not detect any CH_4 and suggested an upper limit of 0.02 ppbv above the planetary boundary layer (F. Montmessin et al. 2021). Even if seasonal variations and day-night concentration differences measured by Curiosity (Webster et al. 2021) can be explained by continuous CH_4 microseepage close to the rover location and atmospheric convection (J. E. Moores et al. 2019a, 2019b), rapid loss processes are required to reconcile both the observed surface CH_4 releases and the global nondetection by TGO.

Suggested fast CH_4 removal mechanisms include triboelectricity (W. M. Farrell et al. 2006; S. K. Atreya et al. 2007), oxidation by UV-activated magnesium perchlorate (X. Zhang et al. 2022), and physical and chemical sequestration in the soil (R. V. Gough et al. 2010; S. J. Knak Jensen et al. 2014). Regarding CH_4 production mechanisms, it has been suggested that CH_4 on Mars could have a biotic (S. K. Atreya et al. 2007; B. P. Weiss et al. 2000) and/or abiotic origins, including hydrothermal processes such as serpentinization (C. Oze & M. Sharma 2005). In addition, CH_4 from both origins could be temporally stored in subsurface reservoirs such as clathrate hydrates (O. Prieto-Ballesteros et al. 2006; B. K. Chastain & V. Chevrier 2007, D. Z. Oehler & G. Etiope 2017). Although the trapping of atmospheric CH_4 in clathrates is negligible under the present-day Martian conditions (C. Thomas et al. 2009; M. G. Trainer et al. 2010), CH_4-rich clathrate hydrates, formed in contact with a subsurface source or under an early Martian atmosphere, are stable in the current cryosphere

(E. Gloesener et al. 2021). Their dissociation is induced by depressurization (erosion, ice sublimation, impacts, seismic events…), temperature increase (magmatic intrusions, seasonal and obliquity variations…), or inhibitor injection (increase of water salinity…). Clathrates formed in the deeper soil layers will not be subject to seasonal variations and will only dissociate on short time scales if exhumation processes or internal thermal inputs occur. However, on longer time scales, it has also been proposed that obliquity variations can lead to clathrate dissociation from near-surface to deeper layers (O. Prieto-Ballesteros et al. 2006; M. J. Root & M. E. Elwood Madden 2012).

Preliminary studies postulated clathrates in the Martian subsurface can form from 15 m down to 24 km deep approximately (M. Max et al. 2011). E. Gloesener et al. (2021) showed that the stability field of CH_4-clathrates in the crust of Mars extends down to 8–12 km in equatorial regions and 14–21 km in high-latitude regions in the presence of pure water. The presence of salts can shift the lower limit of the clathrate stability zone upwards by several kilometers.

In the Gale crater, the pressure and temperature conditions for CH_4-rich clathrate stability are met from ~50 m deep (E. Gloesener et al. 2021). J. Pla-Garcia et al (2019) simulated the transport and mixing of CH_4 in the crater, assuming a CH_4 steady-state release rate consistent with the CH_4 diffusion from shallow clathrate deposits. The study showed that, if the CH_4 source is located inside the crater, the CH_4 atmospheric concentrations fluctuate from 0.1 to ~1 ppbv, comparable to the TLS-SAM's low-background CH_4 abundances.

Mineralogical findings suggested that the Gale crater may have contained an ancient lake. The crater formed during Late Noachian to early Hesperian period (i.e., 3.8–3.6 Ga), whereas subsequent sedimentary strata formation (the clay minerals and sulfate layers) occurred during the Hesperian Period (B. J. Thomson et al. 2011; J. A. Grant et al. 2014; M. C. Palucis et al. 2014; J. P. Grotzinger et al. 2015). In situ detections by the Curiosity rover have revealed a high diversity of sedimentary layers in Mt. Sharp (formally named Aeolis Mons) that record multiple episodes of ancient alteration aqueous processes (e.g., C. N. Achilles et al. 2020) including groundwater activity (M. T. Thorpe et al. 2022). In particular, the coexistence of clay minerals and sulfates was found at high abundances in several drill samples collected from the Murray Formation (T. F. Bristow et al. 2018) and in the Glen Torridon area (M. T. Thorpe et al. 2022). As an example, 35 wt% of collapsed clay minerals, probably smectites, were identified to at least 370 m vertical section in the Murray formation (elevation −4100 to −4500 m; V. M. Tu et al. 2021). In the case of the salts, calcium sulfates (30–50 wt%) were found in a layer 150 m thick (elevation −4200 to −4370 m), and magnesium sulfate (26–36 wt%) was intermittently detected in a layer immersed in the previous thicker one, about 10 m thick (at an elevation of approximately −4300 m; W. Rapin et al. 2019).

The Murray formation was probably buried up to 1 km deep after its formation (J. P. Grotzinger et al. 2015; W. Rapin et al. 2019). When the Murray formation was buried, it was an area conducive to the coexistence of clathrates, clay minerals, and salts. Currently, clathrates can continue to coexist if the layers of clay minerals and salts reach depths under sufficient pressure so that the clathrates are also stable.

Mixtures of clathrates with clay minerals and other components have been extensively studied in recent years, both experimentally and theoretically. In the case of CH_4-clathrates, the increase in concentration of both montmorillonite and kaolinite clays can reduce the clathrate nucleation period. However, a smaller quantity of clathrates is formed (S.-H. Park & G. Sposito 2003; J. Ren et al. 2023; R. Wang et al. 2023). Also, this effect can be altered by the presence of other mineral phases such as quartz sand particles, for example (see X. Wang et al. 2025 and references therein). Previous works have shown that the clay surface, the interlayer cation in swelling clays (2:1 type), the pore space availability, and the presence of other soil compounds (i.e., mixtures of different mineral phases, including phyllosilicates and sulfides, and organic matter), are fundamental factors in determining the kinetics and the volume of clathrates formed (R. B. Lamorena & W. Lee 2008; R. Martos-Villa et al. 2014; T. Park et al. 2014; D. Kim et al. 2015; K. Yan et al. 2019; Y. Li et al. 2020a, 2020b; H. Bian et al. 2021). Y. Tao et al. (2020) recently studied by calorimetry the effect of salinity on the formation of CH_4-clathrates in montmorillonite, observing that the increase in NaCl concentration causes a decrease in both the equilibrium temperature and the clathrate conversion rate of methane. The addition of salt causes fewer water molecules to enter the interlayer space, reducing clay swelling and affecting the amount of clathrate that can form in this interlayer due to the decrease in available water molecules.

The objective of this work was to determine the kinetics of formation and dissociation of ice and CH_4-clathrates when they are in contact with clay minerals immersed in sulfate brines, to evaluate the role of the clathrates as a potential source for the CH_4 detections in Gale. We studied the behavior of clathrates both in pure water and in $MgSO_4$ brines of eutectic composition (17 wt%), in the presence of a swelling clay mineral (montmorillonite) and a nonswelling clay mineral (kaolinite) by means of differential scanning calorimetry (DSC). At the working pressures of this study, i.e., 50 and 100 bar, we were experimentally simulating depths between around 0.5 and 1 km, respectively (E. G. Jones et al. 2011).

2. Methods

The reagents used to prepare the samples were methane gas (CH_4, 99.5% purity, Praxair, USA), magnesium sulfate heptahydrate $MgSO_4{\cdot}7H_2O$ (VWR, Ph. Eur., USA), kaolinite KGa-2 (Warren County, Georgia, USA, The Clay Minerals Society), $Al_2Si_2O_5(OH)_4$ (G. N. White 1992), Ca-montmorillonite STx-1b (Gonzales County, Texas, USA The Clay Minerals Society), $^{[4]}(Si_{7.753}Al_{0.247})$ $^{[6]}(Al_{3.281}Mg_{0.558}Fe_{0.136}Ti_{0.024}Mn_{0.002})$ $^{[12]}(Ca_{0.341}Na_{0.039}K_{0.061})O_{20}(OH)_4$ (K. Emmerich et al. 2009; E. Castellini et al. 2017), and H_2O (Milli-Q water with TOC <5 ppb and resistivity >18 MΩ cm.

The experiments were done in a high-pressure μDSC7 evo calorimeter (Setaram, France), factory-calibrated for temperature and energy using a standard material (ENR7-6ET01, naphthalene LGC 2603) and the Joule effect method, respectively. The errors associated with the measurement of melting temperature and enthalpy, respectively, were ±0.20 K and ±4.3 J g^{-1} (V. Muñoz-Iglesias & O. Prieto-Ballesteros 2021; O. Prieto-Ballesteros et al. 2022). Data have been processed by CALISTO Thermal Analysis Software v1.493 and OriginPro 2019 analysis program. Negative peaks correspond to endothermic processes such as meltings, whereas positive peaks correspond to exothermic processes such as crystallizations.

Table 1
Composition of the Systems Used in Each Set

Set	W (mg)	MS17aq (mg)	Mt (mg)	Kaol (mg)
Run 1				
1) W	81.5	…	…	…
2) MS17aq	…	84 (69.7 H_2O + 14.3 $MgSO_4$)	…	…
3) W + Mt	75	…	50.9	…
4) W + Kaol	81.4	…	…	49
5) MS17aq + Mt	…	85.5 (71 H_2O + 14.5 $MgSO_4$)	51.6	
6) MS17aq + Kaol	…	82.7 (68.6 H_2O + 14.1 $MgSO_4$)	…	50.1
Run 2				
1) W	78.4	…	…	…
2) MS17aq	…	79.1 (65.6 H_2O + 13.4 $MgSO_4$)	…	…
3) W + Mt	74.5	…	51.1	…
4) W + Kaol	87.1	…	…	50.1
5) MS17aq + Mt	…	76.9 (63.8 H_2O + 13.1 $MgSO_4$)	51.5	…
6) MS17aq + Kaol	…	82.6 (68.6 H_2O + 14 $MgSO_4$)	…	48.9

Note. Each set was studied at 100 and 50 bar, using the same sample. W: pure liquid water, MS17aq: $MgSO_4$ 17wt% aqueous solution, Mt: montmorillonite, Kaol: kaolinite.

To study the thermodynamics and kinetics of the systems, we followed a protocol similar to previous works (H. Bian et al. 2021; M. D. Robustillo et al. 2022; approximately 14 hr long), which consisted of three steps: step (1) Cooling at 1 K min^{-1} to 243 K, step (2) 15–20 cycles in the temperature range 243–280 K at 3 K min^{-1}, to favor the recrystallization of the ice formed to clathrate, and, finally, step (3) Heating at 0.2 K min^{-1} up to 303 K. This protocol allowed us to study, on the one hand, the number of cycles and recrystallization time from ice to clathrate (in step 2), and, on the other hand, the temperature and enthalpy of dissociation, and the mass fractions of ice, clathrate, and residual metastable supercooled water formed (in step 3).

Each set of experiments was done at 100 and 50 bar of CH_4 gas, with montmorillonite or kaolinite (approximately 50 mg), in the presence of pure water or eutectic solution of $MgSO_4$ (17wt%; approximately 65–85 mg of H_2O; see the exact composition of each solution used in Table 1). Within each set, the sample was first subjected to 100 bar and then, without changing the sample, the experiment was repeated at 50 bar, in order to also study the "memory effect" of the different systems as well. It should be noted that memory effects may predominate over other variables during clathrate formation, potentially influencing differences in volume or timing of clathrate formation in the second series of experiments. However, dissociation and melting temperatures should not be affected by the memory effect. Runs were repeated twice, assigned as Run 1 and Run 2, to assess the level of the metastability phenomena in the systems at the conditions studied, which is expected to be high (J. D. Toner et al. 2014; V. Muñoz-Iglesias et al. 2019).

3. Results

3.1. Recrystallization and Dissociation Cycles

The recrystallization and dissociation cycles of each set of experiments are described below. The complete description of the runs, including the deconvolution of the peaks in those signals that appear superimposed, can be seen in the Appendix A (Figures A1–A12).

3.1.1. Set 1: H_2O–CH_4

During the recrystallization cycles from ice to clathrate (Figure 1, black lines; Figures A1 and A2), it was observed that the amount of ice decreased in each cycle. In almost all runs done, this recrystallization was most effective up to cycle #7 at both 100 and 50 bar. From this cycle, the recrystallization of ice to clathrate occurred more gradually.

The dissociation temperatures agreed perfectly with the phase diagram (E. D. Sloan & C. A. Koh 2008; Figure 2), both at 100 and 50 bar.

3.1.2. Set 2: $MgSO_4$ 17wt%—CH_4

Interestingly, in the presence of salt (Figure 1, red lines; Figures A3 and A4), the recrystallization from the first cycle (Figure A3) at 100 bar was very effective (the ice peak decreased noticeably from the beginning). However, at 50 bar, the intensity of the ice peak was practically constant throughout the 20 cycles. This is because, at these conditions, clathrates melted at lower temperatures, falling within the temperature range of the thermal cycle (i.e., 243–280 K); thus, in each cycle, the crystallization and subsequent melting of both ice and clathrates were observed.

In the presence of 17wt% $MgSO_4$, in principle, the melting temperatures of ice and CH_4-clathrates should decrease by 4 K and 2 K, respectively (O. Prieto-Ballesteros et al. 2005). At Run 1 at 100 bar, the melting of ice was a small wide asymmetric peak whose T_{onset} (start of the melting) was at 267.1 K and T_{peak} (minimum intensity of the peak) at 269.1 K (W. Lin et al. 2013; Figure A3), agreeing with the $MgSO_4$–H_2O phase diagram (R. Nakamura & E. Ohtani 2011). Clathrate dissociation peaks, in the presence of salt, were less sharp than in pure water (Figure 1). Thus, although T_{onset} appeared at 277 K, 4 K below the theoretical calculations (i.e., 281 K), T_{peak} fit perfectly with the predicted one, appearing at 281 K. This behavior was repeated experimentally in Run 2 (Figure A4). The broadening of the peaks in the presence of sulfate may be related to dynamic gas exsolution processes during the melting, caused by a reduction in gas solubility due to the salting-out effect (A. S. J. Méndez et al. 2017) and/or an increase in the metastability in water-salt-clathrate systems (V. Muñoz-Iglesias et al. 2019). Metastability can temporarily promote the permanence of supercooled brines upon cooling (J. D. Toner et al. 2014) or, conversely, the maintenance of clathrates outside the stability zone upon heating (Y. Li et al. 2021, Y. Wei & N. Maeda 2023).

At 50 bar, a behavior similar to that at 100 bar was observed. The ice melting peak appeared at a temperature around 267 K, close to that indicated by the $MgSO_4$–H_2O phase diagram (Figure A3). However, the clathrate dissociation suffered a slight shift to lower temperatures, with T_{onset} at 273.8 K and T_{peak} at 275.3 K, instead of 277 K indicated by theoretical calculations (O. Prieto-Ballesteros et al. 2005). The

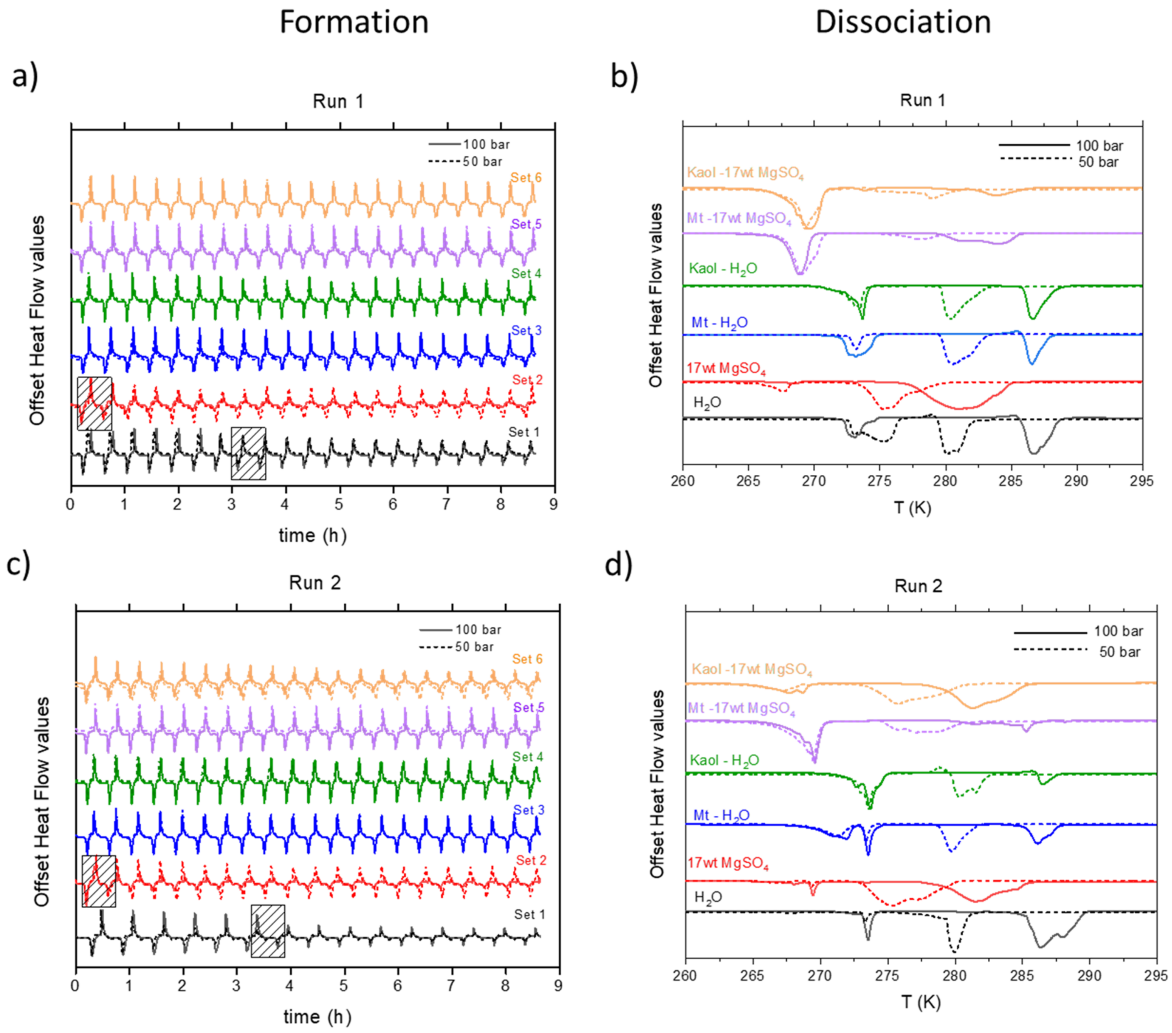

Figure 1. Recrystallization cycles (a), (c) and meltings during heating (b), (d) of the sets 1–6, at 100 and 50 bar. The shadow areas in panels (a) and (c) indicate the mean temperature cycle until which the ice recrystallization to clathrate was efficient in the sets without clay minerals (sets 1 and 2). The presence of clays inhibited this recrystallization (sets 3–6).

difference can be explained by salting-out effects and/or metastable phenomena, similar to the case at 100 bar.

In Run 2 at 50 bar, there was an additional melting at a very low temperature, at 265 K (Figure A4), which could be due to a phase transition in the magnesium sulfate phase or, although less likely, to metastable ice or clathrates. Based solely on the thermogram data, it is not possible to determine this. Then, the ice melting occurred at 269 K, as expected in the presence of 17wt% $MgSO_4$. The main clathrates dissociated at temperatures similar to those observed in Run 1 under both pressures (281.5 (T_{peak}) K at 100 bar, and 275.2 (T_{peak}) K at 50 bar) (Figure A4).

3.1.3. Set 3: H_2O–Mt–CH_4

In the presence of montmorillonite (Figure 1, blue lines; Figures A5 and A6), the recrystallization of ice to clathrate appeared to be inhibited, with the ice peak decreasing less over the 20 cycles.

In Run 1 (Figure A5), only one clathrate dissociation peak was measured, whose T_{onset} coincided with the system without clay, i.e., H_2O–CH_4 (set 1). This may be because the layer charge of montmorillonite, which prevented clathrate formation near the clay surface (Y. Li et al. 2020a). Clathrates are preferentially formed from water molecules that are far from the clay surface and therefore not strongly bound to it. In other words, most of the clathrates were formed in the bulk. Y. Sun et al. (2021) observed this behavior experimentally in CO_2 clathrates.

In Run 2 (Figure A6), the ice peak split. The first peak appeared at 269.4 K. As in the previous set, it was not possible to know from the data whether that contribution was caused by ice or metastable clathrate melting. Metastability can contribute to creating emptier clathrates (P. G. Lafond et al. 2015; R. Sun et al. 2020) or letting fluids remain temporary in liquid state, as supercooled aqueous solutions, outside its stability zone (J. D. Toner et al. 2014). The main clathrate dissociation occurred at a similar temperature to that in Run 1, at 285.9 K.

3.1.4. Set 4: H_2O–Kaol–CH_4

The presence of kaolonite, like montmorillonite, also appeared to inhibit recrystallization of ice to clathrate (Figure 1, green lines; Figures A7 and A8).

In Run 1 (Figure A7), only one clathrate dissociation peak was observed, whose T_{onset} matched the H_2O–CH_4 system at both 100 and 50 bar, i.e., set 1. Occasionally ice and/or clathrate peaks appeared as broad signals made up of two

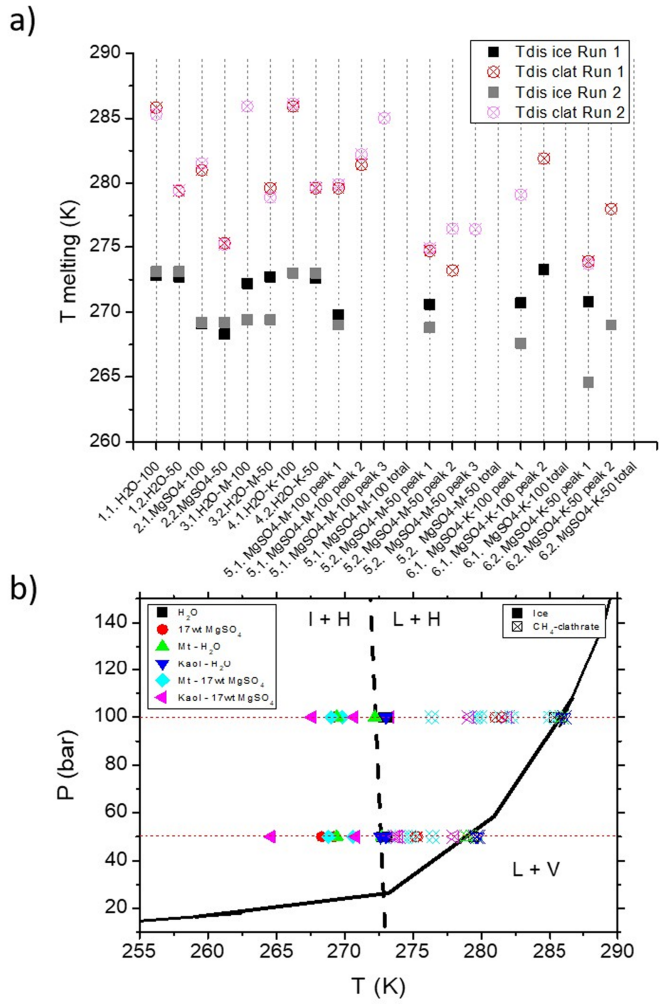

Figure 2. (a) Ice and CH_4 clathrate melting temperatures, and (b) H_2O–CH_4 phase diagram with the experimental temperatures shown in panel (a). L: liquid aqueous solution, I: water ice, H: CH_4-clathrate hydrate, V: CH_4 gas. The composition of each set can be seen in Table 1.

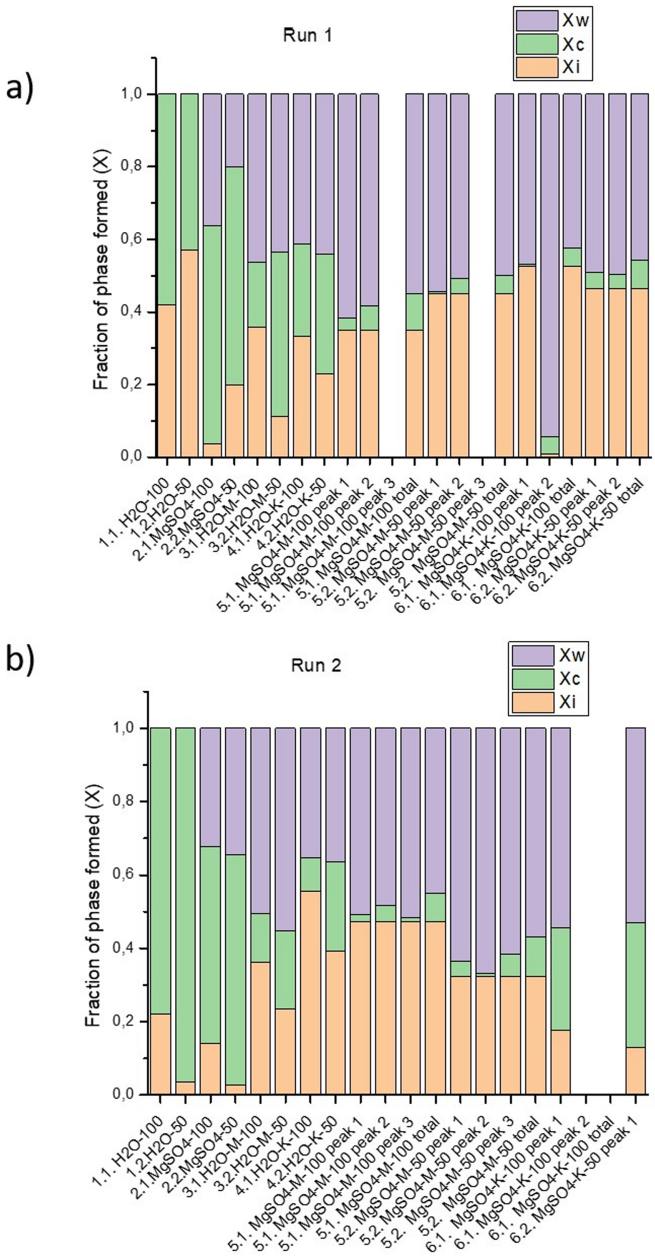

Figure 3. Fraction of ice (Xi), clathrate (Xc), and residual supercooled water (Xw) formed in each set. The composition of each set can be seen in Table 1.

contributions (Figures A7 and A8). This may be related to the occurrence of two nucleation/dissociation events, one on the siloxane surface of kaolinite and one in the bulk (Y. Li et al. 2020b).

Unlike the effect of salt ($MgSO_4$), whose ions generate electrolytic forces that decrease the melting temperature of both ice and clathrate, clay minerals do not seem to affect it (Figure 2). However, they did affect the amount of clathrates formed, decreasing it (Figure 3, Section 3.2).

3.1.5. Set 5: $MgSO_4$ 17wt% - Mt - CH_4

The addition of salt to the montmorillonite system did not appear to promote recrystallization from ice to clathrate (Figure 1, purple lines; Figures A9 and A10).

In Run 1, the ice melted around 269 K (Figure A9), in agreement with the H_2O–$MgSO_4$ phase diagram (R. Nakamura & E. Ohtani 2011). In the case of the clathrate melting, a broad peak with two contributions was observed, one at 279.6 K and another at 281.4 K. In comparison with H. Bian et al. (2021), who worked with mesoporous and macroporous silica particles, and according to D. Kim et al. (2015) who studied the effect of pore dimension on clathrates formed in montmorillonite, the dissociation peak at lower temperature corresponded to the melting of more confined clathrates, as those located inside the interlayer space, while the second peak corresponded to clathrates formed outside the interlayer. However, it must be taken into account that the studies mentioned were done in the absence of salt.

Clathrate dissociation temperatures were higher than in the same system without clay mineral (set 2.1), which was 277.2 K (Figure 2).

In Run 2 (Figure A10), like Run 1, the ice peak appeared at 269 K, as it should occur in a solution at 17wt% $MgSO_4$ (Figure 2). The clathrates partially dissociated in three steps, at 279.9, 282.2, and 285 K.

3.1.6. Set 6: $MgSO_4$ 17wt%–Kaol–CH_4

Similar to what happened with montmorillonite, the addition of salt to the kaolinite system did not appear to promote

recrystallization from ice to clathrate (Figure 1, yellow lines; Figures A11 and A12).

As in the absence of salt (set 4), in Run 1 (Figure A11) the thermograms suggested the existence of two environments. One where ice and clathrates melted at 269 K and 279.1 K, respectively, and another where the ice and clathrates melted at higher temperatures, i.e., at 273 K and 281.9 K, respectively.

In Run 2 (Figure A12), a melting peak occurred at very low temperature, at 265 K. As in the cases mentioned above, it is not possible to know from our data whether it was ice or metastable clathrates. The ice melting peak was then observed at 269 K, as expected in the presence of 17wt% $MgSO_4$. The main peak of clathrates occurred at similar temperatures than in Run 1, (about 280 K at 100 bar and 273 K at 50 bar).

3.2. Enthalpy and Mass Fraction Calculations

From the thermograms, it is possible to calculate the enthalpy of clathrate dissociation (ΔHsc), and the mass fraction of ice (Xi), clathrates (Xc), and residual water (which refers to the water that remained supercooled, in liquid state, without forming ice or clathrates) (Xw) formed (Figure 3). For these calculations, we follow procedures similar to V. Muñoz-Iglesias & O. Prieto-Ballesteros (2021).

Starting with the runs in pure water (set 1), first, we calculated the amount of water ice formed (Equation (1)). Then, the CH_4-clathrate specific enthalpy in pure water, at both 100 and 50 bar, was determined using Equations (2) and (3):

$$\mathrm{mi} = \frac{\Delta \mathrm{Hi}}{\Delta \mathrm{Hsi}} \tag{1}$$

$$\mathrm{mc} = \mathrm{mt} - \mathrm{mi} \tag{2}$$

$$\Delta \mathrm{Hsc(in\ \ pure\ \ water)} = \frac{\Delta \mathrm{Hc}}{\mathrm{mc}}, \tag{3}$$

where "ΔHi" is the melting enthalpy of ice measured by the calorimeter without mass normalization, "ΔHsi" is the specific melting enthalpy of ice (i.e., 333 J g^{-1} in the system with pure water), "mi" is the ice mass, "mt" is the total mass of the initial aqueous solutions, "mc" is the clathrate mass, "ΔHsc(in pure water)" is the clathrate specific enthalpy in pure water, and "ΔHc" is the total enthalpy of the clathrate melting without mass normalization.

In the presence of $MgSO_4$ and/or clay minerals (sets 2–6), a supercooling phenomenon is common (F. González Sánchez et al. 2008; T. Kozlowski 2011; J. D. Toner et al. 2014). In the runs with $MgSO_4$ at 17wt%, the "ΔHsi" used was 226 J g^{-1} (O. Prieto-Ballesteros et al. 2022). To calculate the amount of residual water ("mw") in these runs, we employed the following procedure: Once we obtained "mi" and "mc" using the corresponding ΔHsi and ΔHsc(in pure water) determined in the initial runs in pure water (see Equations (1)–(3)), "mw" was then calculated by the difference between the "mt" and "mi + mc." Thus, the procedure for the systems with salts and/or clay minerals followed Equations (4)–(6):

$$\mathrm{mi} = \frac{\Delta \mathrm{Hi}}{\Delta \mathrm{Hsi}} \tag{4}$$

$$\mathrm{mc} = \frac{\Delta \mathrm{Hc}}{\Delta \mathrm{Hsc(in\ \ pure\ \ water)}} \tag{5}$$

$$\mathrm{mw} = \mathrm{mt} - \ (\mathrm{mi} + \mathrm{mc}). \tag{6}$$

We used ΔHsc in pure water obtained at 100 bar for the calculations of the runs at that pressure, and ΔHsc in pure water obtained at 50 bar for the other runs at that pressure. The complete raw data obtained from the thermograms and the calculations can be found in Table B1 of the Appendix B. It is important to clarify that, due to the use of the enthalpy of dissociation of the clathrate in pure water, assuming a low influence of salinity or mineral surfaces on ΔHsc, these calculations involve a certain degree of uncertainty. Both electrolytic effects and interfacial interactions influence the cage occupancy level and, consequently, the final energy of dissociation. Future experiments, using additional techniques such as X-ray diffraction (XRD) and Raman/infrared spectroscopy, will help us better address this level of uncertainty. A good set of experiments to address this question could consist of measuring CH_4 clathrates formed over a wide range of CH_4 gas pressures (e.g., 20–200 bar) in pure water using DSC, XRD, and Raman spectroscopy. Thus, using XRD and Raman spectroscopy, we can evaluate the cage occupancy level (e.g., C. Petuya et al. 2020; W. Cai et al. 2022) and associate the value at each pressure with the corresponding ΔHsc measured in the DSC.

Overall, in set 1, the measured clathrate dissociation enthalpies were within the range of values provided by previous works (E. D. Sloan & C. A. Koh 2008; M. D. Robustillo et al. 2022), i.e., between 50 and 70 KJ mol^{-1} (to compare with our data in J g^{-1}, considering CH_4-clathrates fully occupied with formula $CH_4{\cdot}5.75H_2O$ and molecular weight 119.5 g mol^{-1}, the reference values correspond to 418–585 J g^{-1}; see Table B1 of the Appendix B). In Run 1, the obtained ΔHsc were 526.5 and 449.8 J g^{-1}, at 100 bar and 50 bar, respectively; in run 2, the obtained ΔHsc were 481.1 and 167.6 J g^{-1}, at 100 bar and 50 bar, respectively. The run 2 at 50 bar gave a ΔHsc value very low, which we attributed to disequilibrium and metastable phenomenon, also common in clathrates (E. D. Sloan & C. A. Koh 2008, V. Muñoz-Iglesias et al. 2019). We did not use that enthalpy to perform the subsequent calculations to obtain the residual water in the presence of $MgSO_4$ and/or clays; instead, we used the enthalpy obtained at that pressure in Run 1.

4. Discussion

4.1. General Trends in Recrystallization Cycles

Recent studies indicate that clay minerals promote the formation kinetics of the initial clathrates formed in the first cooling, before starting the recrystallization cycles (S.-H. Park & G. Sposito 2003; J. Ren et al. 2023; R. Wang et al. 2023). In our experiments, the initial cooling of all systems resulted in the formation of both ice and clathrates.

In the subsequent formation cycles, involving the recrystallization of the remaining ice into new clathrates, we observed that: if there was only H_2O (set 1), the recrystallization of ice to clathrate was favorable; when adding $MgSO_4$ (set 2), recrystallization continued to occur, even in a more favorable form (i.e., less thermal cycles were necessary to complete the recrystallization); in the presence of clay minerals, both montmorillonite and kaolinite, (sets 3 and 4) recrystallization was inhibited; and in clay minerals, there is also inhibited recrystallization in the presence of salt (sets 5 and 6). This inhibitory effect was greater in montmorillonite than in kaolinite.

This behavior of clays at low temperatures, when ice/salt hydrates are already present, is very interesting. Our experiments show that the promoting effect during the first cooling (when starting from a high temperature where ice or hydrated salts have not yet formed) disappears at low temperatures. The promoting effect is related to the fact that clay surfaces act as condensation points. However, at low temperatures, they appear to contribute to the stability of the ice, preventing it from recrystallizing into clathrate during thermal cycles (contrary to what occurs in their absence).

4.2. Distribution of the Solid Phases in Systems with Clays after Final Cooling

The results with the water-clay mineral systems (sets 3 and 4) suggested that under the conditions used (i.e., with an excess of water with respect to the amount of clay mineral (see Table 1 in Section 2)), most of the clathrate was formed in the bulk, since only a clathrate melting peak was measured at the higher temperatures. Furthermore, this melting occurred at the same temperature as in the absence of salt and clay minerals (set 1). A reasonable approach is to assume that, in systems with clays, clathrates formed in the bulk, where they are less affected by interactions with the charged surfaces of silicates, exhibit thermodynamic behavior similar to that of clathrates formed in pure water. In contrast, within the clay interlayer, confinement and interactions with charged surfaces are expected to change the clathrate thermodynamic behavior. Therefore, in our experiments, it can be hypothesized that the calorimetric signal corresponds mainly to clathrates formed in the bulk, while only a negligible fraction forms in the interlayer or in contact with silicate surfaces.

(1) But what happens when $MgSO_4$ is added?

The cation exchange between Ca^{2+} and Mg^{2+} in montmorillonite depends on the brine concentration and is more favorable at higher concentrations (D. L. Suarez & M. F. Zahow 1989; C. Geyer et al. 2023). However, we assumed that the primary salts formed were hydrated magnesium sulfate ($MgSO_4$) salts, such as epsomite ($MgSO_4{\cdot}7H_2O$) and meridaniite ($MgSO_4{\cdot}11H_2O$), because the number of moles of Mg^{2+} in our experiments was greater than that of Ca^{2+}.

The presence of salts causes fewer water molecules to enter the interlayer. This is due to the water potential gradient between the interlayer space and the bulk solution, which is smaller in saline solutions than in pure water (L. Sun 2016).

(2) How is salt distributed when the system freezes?

M. Yesilbaş (2018) and M. Yesilbaş et al. (2018) showed how ice and hydrohalite ($NaCl{\cdot}2H_2O$) are distributed in montmorillonite both at low and high salt concentrations (which would be the case studied in this work, since we are working with eutectic composition). The works showed that when an aqueous solution of NaCl is frozen in the presence of clay mineral, 3D honeycomb structures are formed, whose walls are composed of clay aggregations in a face-to-face configuration. Clay flocculation is induced at high salt concentrations, increasing the size of the voids between the clay aggregates. The ice crystallizes within these spaces, while the salt is pushed to the surfaces of the clay aggregates where the hydrohalite grows. However, it is important to note that these studies were conducted in the absence of clathrates. Assuming that $MgSO_4$ could behave similarly than NaCl, the hydrated magnesium salt, epsomite ($MgSO_4{\cdot}7H_2O$) and/or meridianiite ($MgSO_4{\cdot}11H_2O$), probably grew on the clay surfaces in the case of our experiments. It should be noted that $MgSO_4$ has multiple states of hydration and can undergo phase changes when heated/cooled or when the water activity in the system changes. As such, its interaction with the clay's surfaces is likely to be more complex than that observed with NaCl. In fact, additional small low-temperature fusions have sometimes been observed with $MgSO_4$ present in the experiment (see Appendix A).

Therefore, we must treat the assumption that $MgSO_4$ behaves similarly to NaCl as a potential hypothesis for now, rather than a proven mechanism. Future experiments in the absence of clathrates, using only $MgSO_4$-clay systems, may help to better measure this other uncertainty.

All of those observations related to the distribution of the salt in the clay systems above and below the freezing point can be extrapolated to our more complex experiments, that is, sets 5 and 6 (i.e., clat + MS17 + Mt, and clat + MS17 + Kaol, respectively). Thus, in the first case with montmorillonite, in principle, the formation of clathrates within the clay interlayer space may be more favorable than in the saltier bulk. Therefore, a possible interpretation of the thermograms of Run 1 of set 5 is that the clathrates that dissociated first at a lower temperature (i.e., 279.6 K) were those that formed in the bulk (with higher salt concentration), while clathrates that dissociated at higher temperature (i.e., 281.4 K) were those that formed in the interlayer.

In summary, comparing the behavior of clathrates in clays in the absence and presence of salt shows that: (i) In the absence of salt, the most confined clathrates (within the pores of porous silica particles or in the interlayer of montmorillonite) dissociated earlier than those found between particles (D. Kim et al. 2015; H. Bian et al. 2021); (ii) In the presence of salt, according to our experiments, the interpretation of the dissociation temperatures could be contrary to that obtained in the absence of salt, likely due to the higher concentration of salt in the bulk than within the interlayer. In other words, depending on the ratio between the different compounds in the salt-clay system, the thermodynamic behavior and spatial distribution of clathrates will depend on the balance between intra- and interparticle confinement and the distribution of salt ions.

In the presence of salt, it must be considered that the amount of clathrates formed in the interlayer decreases with respect to the case in pure water due to osmotic effects (Y. Tao et al. 2020). Another plausible interpretation is that we may not be observing clathrates from the montmorillonite interlayer (in the systems without salt, i.e., sets 3 and 4, it was not seen either), but clathrates formed at the clay surface (corresponding to the peak at lower temperature, peak 1), with salt adhered, and clathrates formed in the bulk (corresponding to the peak at higher temperature, peak 2).

In run 2 of set 5 (clat + MS17 + Mt), it was possible to distinguish the clathrates formed on the surface (environment more enriched with salt, which adheres to the walls; M. Yesilbaş 2018), the clathrates formed in the bulk (with less salt than the surface), and the clathrates formed in the interlayer (with less salt than the bulk; L. Sun 2016).

On the other hand, the thermogram of Run 1 of set 6 (clat + MS17 + Kaol) fits very well with what was observed by Y. Li et al. (2020b), where it is mentioned that clathrates in the presence of kaolinite can undergo two nucleation events, one

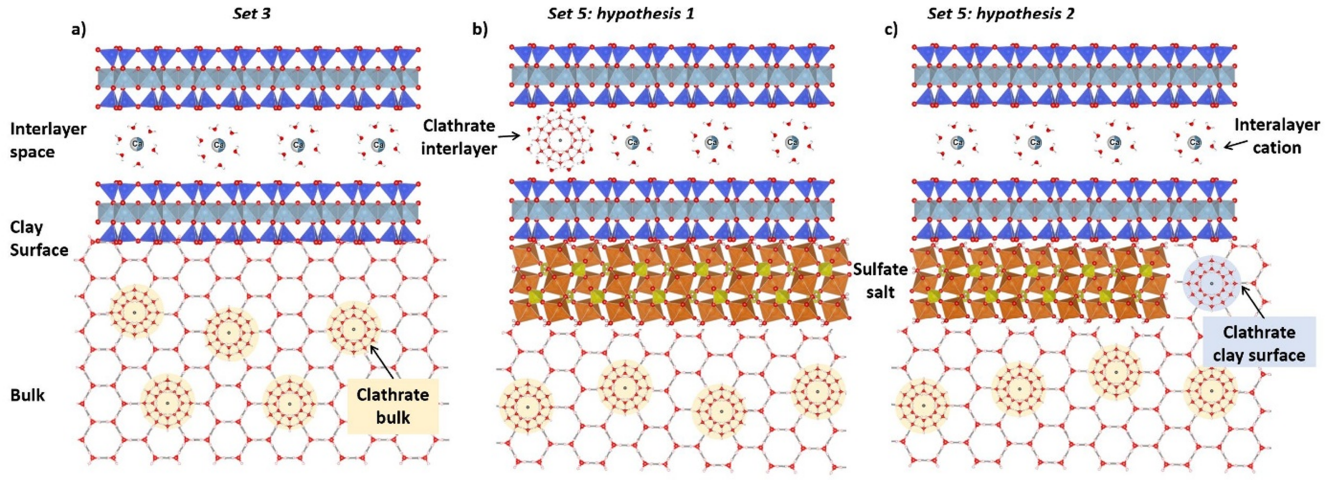

Figure 4. Schematic representation of the hypothetical final situations of the systems with montmorillonite. (a) Set 3 H_2O–Mt–CH_4: where the only melting peak of clathrate is related to those formed in the bulk (Figures A5 and A6), (although we cannot exclude the presence of minor amounts of clathrate formed in the interlayer); (b) Set 5 $MgSO_4$ 17wt%–Mt–CH_4, hypothesis 1: assuming that the first melting clathrate peak (peak 1) is related to those located in the bulk and the second (peak 2) in the interlayer (Figures A9 and A10); (c) Set 5 $MgSO_4$ 17wt%–Mt–CH_4, hypothesis 2: assuming that the first clathrate melting peak (peak 1) is related to those located on the clay surface and the second one (peak 2) in the bulk (Figures A9 and A10)

on the surface and the other in the bulk. Combining this observation with the study of M. Yesilbaş (2018), where it is demonstrated that the salt is concentrated on the surface, the most likely interpretation of our thermograms is that peak 1 corresponded to the clathrates formed on the surface of the kaolinite, and peak 2 to the clathrates formed in the bulk, since kaolinite has no interlayer (see, for instance, Figure 1 of S. Tamamura et al. 2014).

We illustrate the hypothetical end-situation of montmorillonite experiments in Figure 4. To determine which hypothesis is correct, it will be necessary to repeat the experiments, monitoring them with other techniques that identify changes in the environment of each molecule, such as Raman/infrared spectroscopies and XRD (e.g., C. Gil-Lozano et al. 2020, V. Muñoz-Iglesias et al. 2021).

4.3. Dissociations

1. In set 1 (with pure H_2O), the dissociation temperatures perfectly matched the phase diagram (Figure 2(b)), both at 100 and 50 bar.
2. In set 2 (with 17wt% $MgSO_4$), ice melting occurred at 269 K, as indicated by the H_2O–$MgSO_4$ phase diagram (R. Nakamura & E. Ohtani 2011). The clathrate dissociation peak, at 100 bar, was broader than in the absence of salt, having a T_{onset} (initial melting) slightly lower than the theoretical predictions ($\Delta T \approx 4$ K), but the T_{peak} (intensity minimum of the peak) matched the theoretical values (O. Prieto-Ballesteros et al. 2005). However, at 50 bar, the T_{peak} fell 2 K below the theoretical predictions. This discrepancy is likely probably because the experimental clathrates were not 100% occupied, being less stable and more sensitive to the electrolytic forces of the saline ions that attract the H_2O molecules, causing clathrate dissociation at lower temperatures.
3. The dissociation temperatures in sets 3 and 4 (i.e., with clay minerals but without salt) of both ice and clathrates coincide with those observed in set 1. Unlike the effect of salt ($MgSO_4$), clay minerals seem to reduce the amount of clathrates formed (due to the strong bonding of part of the water molecules to the clay surfaces), but not the dissociation temperature. Additionally, we observed that the inhibition effect on clathrate hydrates seems more important for kaolinite than montmorillonite, although some metastability can occur occasionally (Figure 3). To visualize these observations clearly, Figure 5 shows the comparison of the initial aqueous solution and the clay mineral fractions at the beginning of each experiment with the final clathrate fraction formed upon cooling.
4. In set 5, the distribution of $MgSO_4$ salt in the Mt–H_2O system created two environments. One possible interpretation is that one corresponded to clathrates formed in the interlayer (or perhaps on the outer surface of the clay), and the other was the clathrates in the bulk. Thus, with montmorillonite, both at 100 and 50 bar, one possible interpretation is that the amount of clathrates formed in the bulk (peak 1) was lower than that of the clathrates formed in the interlayer (peak 2), due to the salting-out effect (Figure 3).
5. In the case of set 6, with kaolinite, there were also two environments where clathrates formed, but in this case, unequivocally, since kaolinite lacks an interlayer space, one corresponding to the clathrates formed on the surface of the clay, with salt adhered, and the other was the clathrates in the bulk, more diluted. At 100 bar, the amount of clathrates formed on the surface (in this case, peak 1), was lower than that formed in the bulk (in this case, peak 2) since the salt was concentrated on the surface.
6. Another possible interpretation for the meltings observed in set 5 is that we observed the clathrates formed on the surface but not inside the interlayer (in the systems without salt it was not seen either). Consequently, the interpretation for both clays, montmorillonite and kaolinite (sets 5 and 6), is that the Peak 1 was due to the clathrates formed on the surface, with salt adhered, and peak 2 was the clathrates formed in the bulk, with the diluted solution.

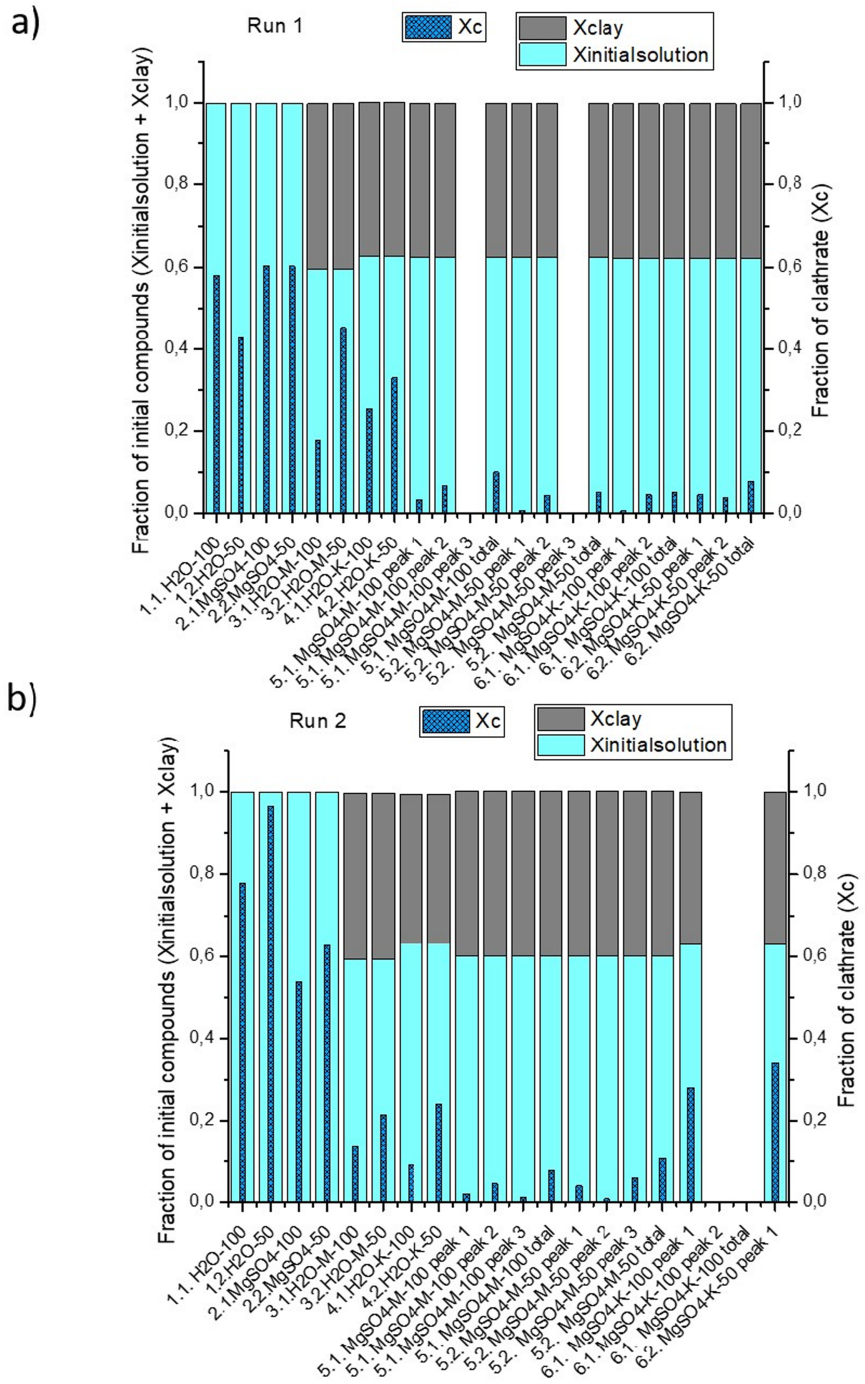

Figure 5. Initial fractions of clay minerals and aqueous solution at the starting of each experiment (gray and light-blue columns, respectively) and final fraction of clathrates formed upon cooling (dotted dark-blue columns). The composition of each set can be seen in Table 1.

4.4. Implications on Mars: Gale Crater

Considering both the global history of Mars (V. Chevrier & P. E. Mathé 2007) and the local history of the Gale crater (J. P. Grotzinger et al. 2015), clay minerals were formed during the Noachian, by both hydrothermal water and surface waters. Subsequently, the acidification of the environment due to an increase in volcanic activity during the Hesperian, and the loss of the atmosphere, allowed sulfates to precipitate. During this period, sediments were deposited, possibly up to 1 km high over the Murray formation (W. Rapin et al. 2019). Thus, the pressurization of the clay and sulfate layers in contact with groundwater could have facilitated the stabilization of clathrates, assuming that there was a CH_4 supply from the interior.

Our data indicate that the amount of CH_4-clathrates stabilized in coexistence with clay minerals and sulfates could be low. Therefore, clathrate deposits at the Gale crater could have been sparse and stored much less CH_4 during the Hesperian due to their inhibited formation in contact with clay minerals and sulfates. This claim is also valid for other Martian regions with sedimentary layers with high amounts of sulfates and clay minerals.

Currently, CH_4-clathrates at the Gale crater can be stable at depths where they are not affected by seasonal temperature fluctuations (E. Gloesener et al. 2021). However, methane could have slowly been released from buried clathrate over geologic time scales as the gradual erosion of overburden made them shallow enough to be thermally dissociated by climatic variations. Heat flux inputs from the interior, seismic activity, or impacts, could also contribute to the localized and episodic dissociation of clathrates and subsequent gas release. The final distribution of the clathrate deposits depends strongly on whether they form in contact with clay-rich sediments.

Another interesting topic for present times is the stabilization of CO_2-clathrates at layers close to the surface, since they can form at lower pressures than CH_4-clathrates (J. Longhi 2006; E. D. Sloan & C. A. Koh 2008). It has been demonstrated that with just a two-cycle formation method, the conversion of ice to CO_2-clathrate can be favorable in presence of $MgSO_4$ salt, even at pressure and temperature ranges close to surface conditions (i.e., 5–20 bar and 90–245 K; see Figure 6 of E. Safi et al. 2017). However, clay minerals may have a similar effect on CO_2 clathrates as on CH_4 clathrates (e.g., A. Botan et al. 2010; D. Kim et al. 2015; Y. Sun et al. 2021; Y. Li et al. 2022). Future experiments using a similar methodology to that used in this work but with CO_2 instead of CH_4 will help to address the role of clays and sulfates in formation and dissociation of CO_2 clathrates under subsurface Martian conditions, and then better understand their role in the past and present Martian atmosphere.

5. Conclusions

In this work, the kinetics of formation and dissociation of CH_4 clathrates in the presence of $MgsO_4$ brines and two types of clays, montmorillonite (swelling clay mineral) and kaolinite (nonswelling clay mineral), were studied by differential scanning calorimetry. The experiments indicate that the mineralogy of the sediments in which clathrate hydrates form significantly affects their formation kinetics and eventually their total storage capacity. The results showed that clathrate growth can be strongly inhibited in contact with clay minerals and sulfates brines (see Figure 5). However, since clathrates may form within clay interlayers or other highly confined pore spaces, DSC measurements alone may not fully capture their occurrence or stability. To obtain a more comprehensive assessment in future experiments, we will combine calorimetry with analytical techniques that can monitor and quantify cage occupancy, such as XRD, Raman spectroscopy, and IR-spectroscopy.

Mineralogy is a key parameter for evaluating the amount of methane potentially released from clathrate dissociation on Mars. These data provide new insights to the hypothesis that part of the CH_4 detected on Mars may come from the dissociation of subsurface clathrates (B. K. Chastain & V. Chevrier 2007; D. Z. Oehler & G. Etiope 2017; E. Gloesener et al. 2021). Specifically, the studied mineral association has direct application for the Gale crater, where Curiosity measurements confirmed the presence of fluvial-deltaic deposits formed by both clay minerals and sulfates (J. P. Grotzinger et al. 2015; T. F. Bristow et al. 2018; W. Rapin et al. 2019; V. M. Tu et al. 2021; M. T. Thorpe et al. 2022), as well as CH_4 emissions from the ground (C. R. Webster et al. 2015, 2018). While only the presence of sulfates may contribute to a favorable fast conversion of ice to CH_4-clathrate (this fact was also observed by previous works; E. Safi et al. 2017, 2019) for CO_2-clathrates in the presence of sulfate or chloride solutions, where clathrates were efficiently synthesized with only two thermal cycles), clay minerals affect the crystallization of clathrates, leading to the formation of lower amounts. Thus, the results suggest that clathrate reservoirs within the mineral associations identified in the Gale crater may be relatively sparse, implying that clathrate dissociation during the crater's exhumation would likely have produced only limited CH_4 emissions to the atmosphere. Future investigations combining experimental studies of clathrate formation and kinetics with thermodynamic modeling, methane detections, and geological context will be essential to better constrain the origin and evolution of methane at the Gale crater.

Acknowledgments

The authors would like to thank two anonymous reviewers for their detailed review, which has improved the quality of this work. V.M.-I. acknowledges support from the Marie Curie Postdoctoral Fellowship program (HORIZON-MSCA-2022-PF-01), grant No. 101105979—SECRECY; and the RYC2024-050522-I grant, funded by MICIU/AEI/ 10.13039/501100011033 and the ESF+. C.G.-L. acknowledges support from SOS-Mars project (PID2020-119412RJ-I00) from MICINN Spain. O.P.-B. acknowledges support from the MCIN/AEI/ http://doi.org/10.13039/501100011033 projects PID2022-142490OB-C31, and PCI2023-145992-2. Part of this work has been conducted at the Jet Propulsion Laboratory, California Institute of Technology, under a contract with the National Aeronautics and Space Administration. Government sponsorship is acknowledged.

Appendix A

Figures A1–A12 show the separate thermograms, both the initial temperature cycling phase (left-hand panels) and the final slow heating phase (right-hand panels), of all of the runs (Runs 1 and 2) of the sets studied, at 100 and 50 bar. In each thermogram, the melting temperatures and the deconvolution of the peaks discussed in the main text are indicated.

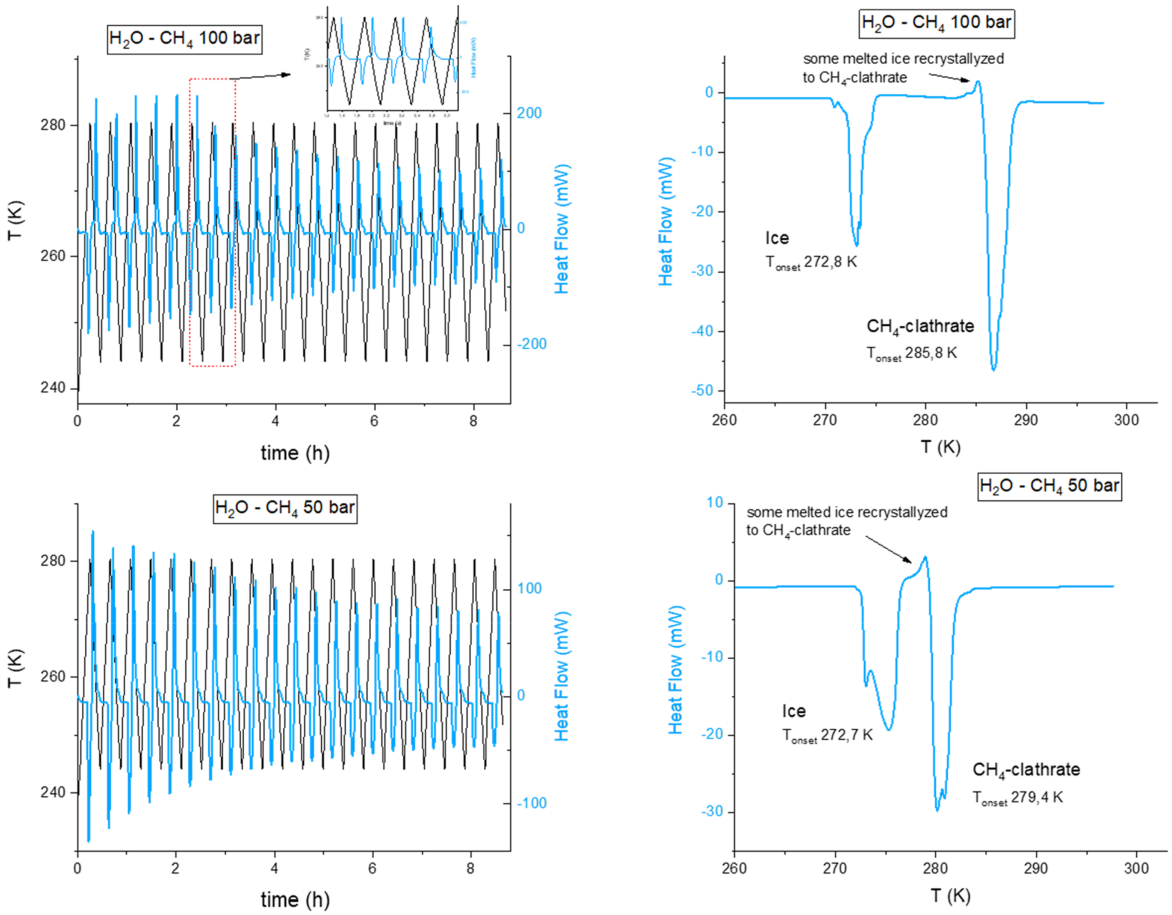

Figure A1. H_2O–CH_4 Run 1.

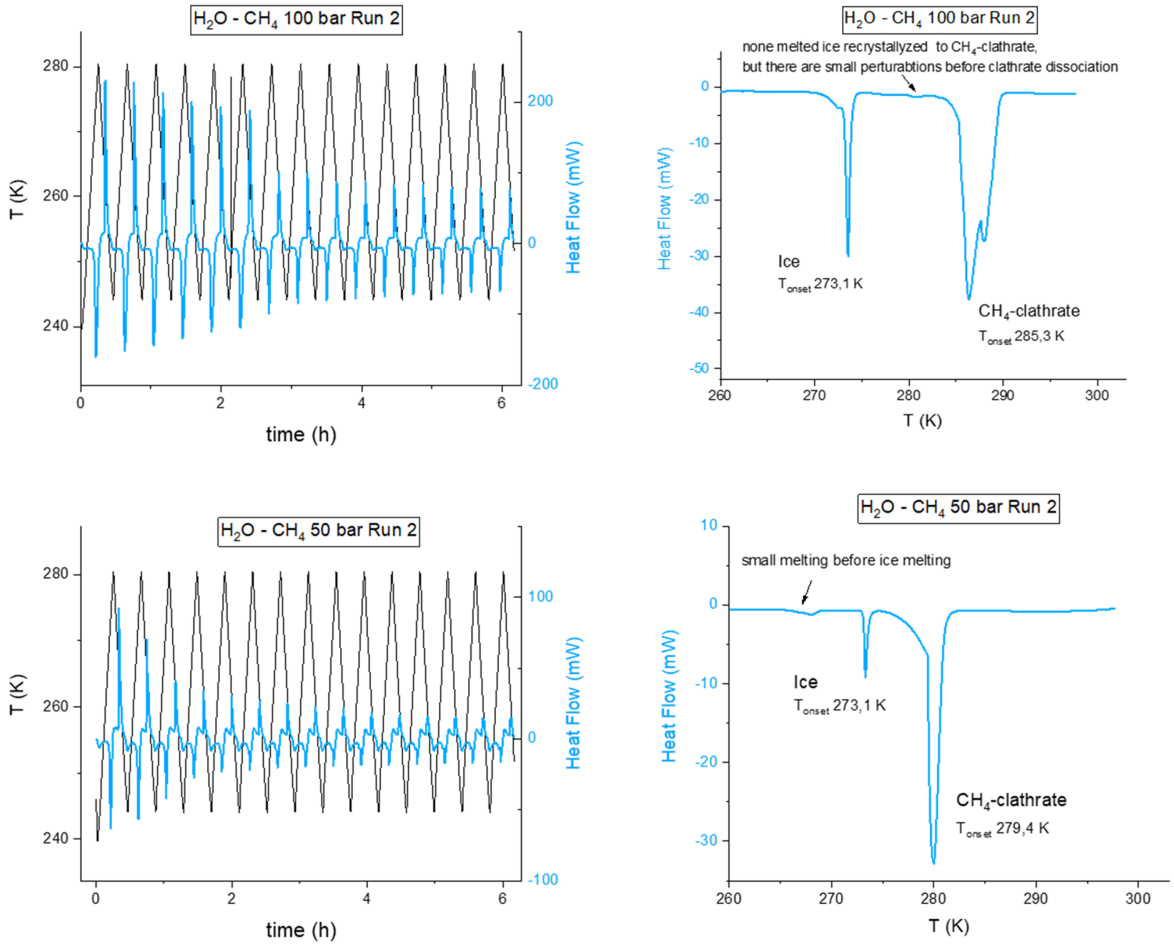

Figure A2. H_2O–CH_4 Run 2.

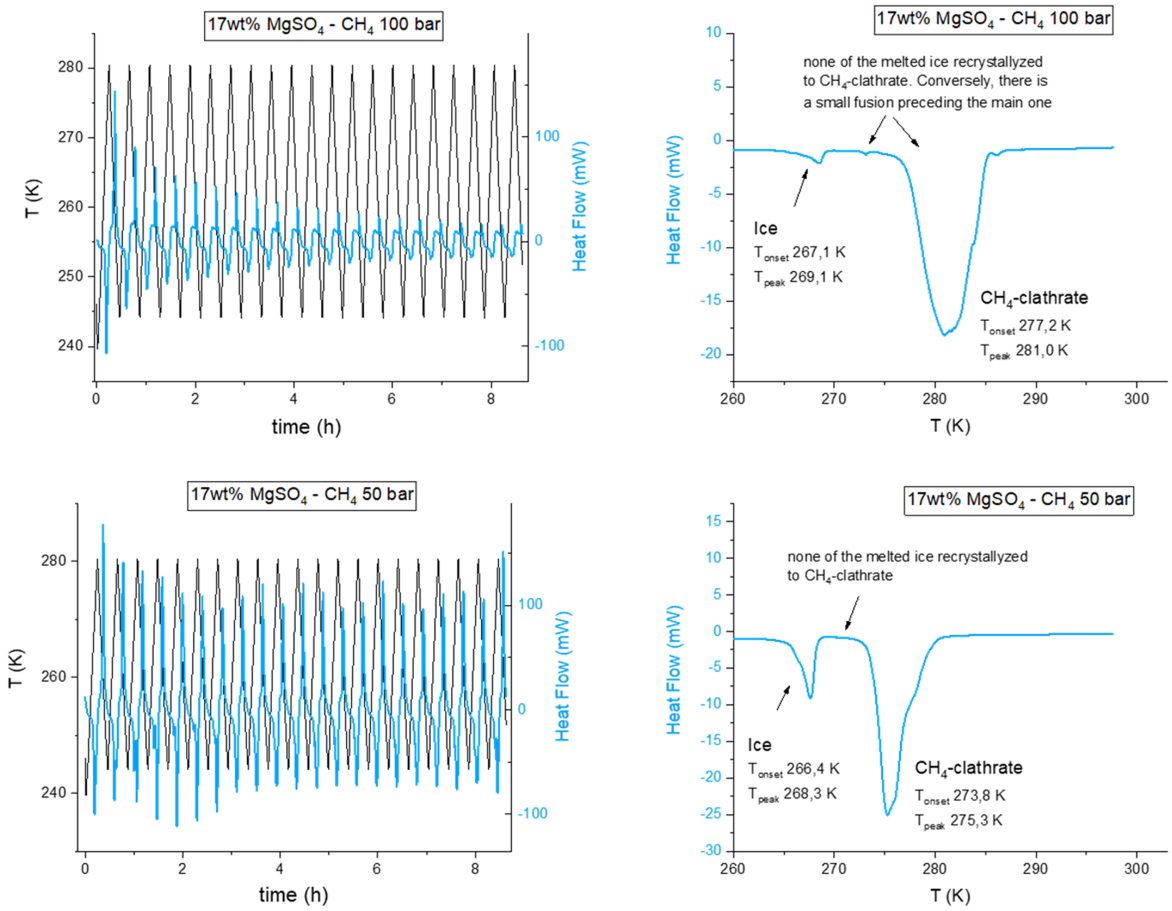

Figure A3. 17wt% $MgSO_4$–CH_4 Run 1.

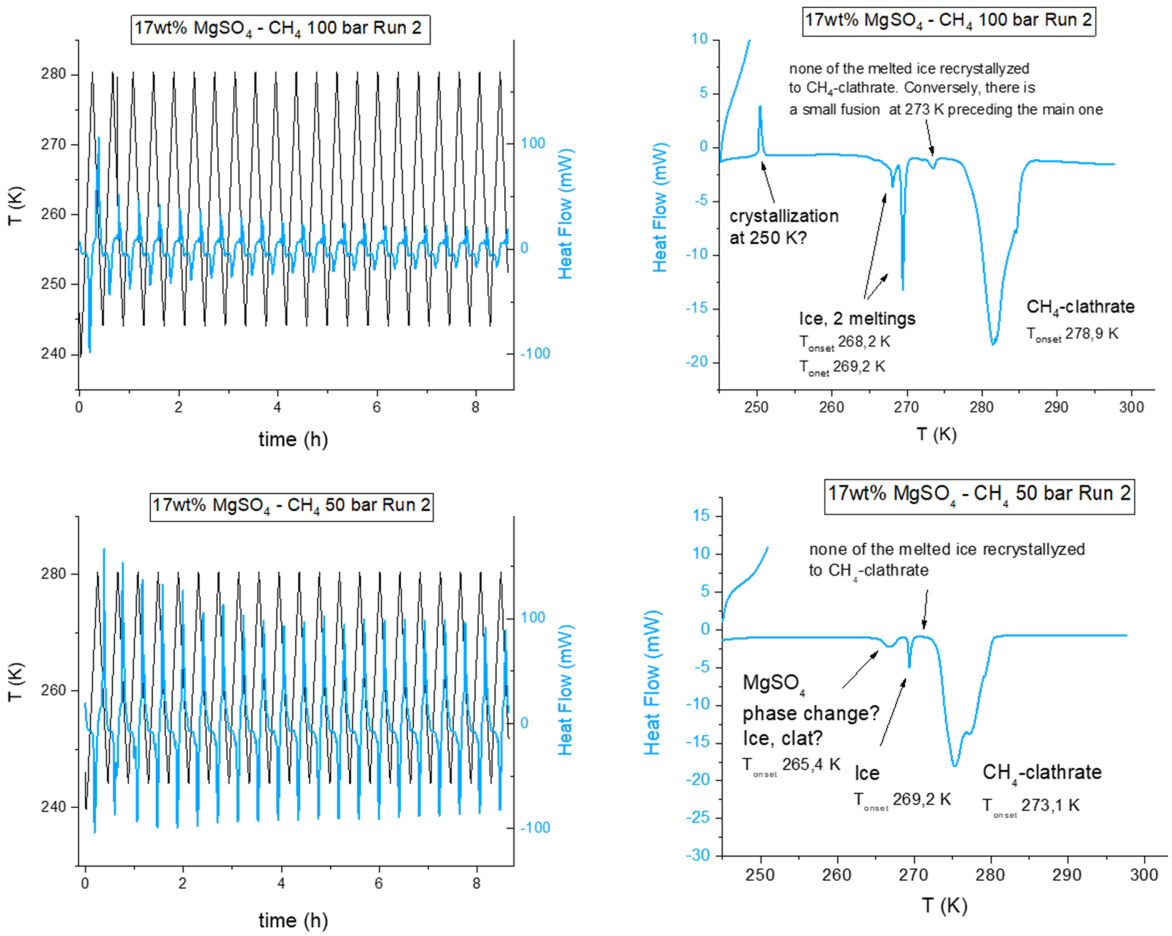

Figure A4. 17wt% $MgSO_4$–CH_4 Run 2.

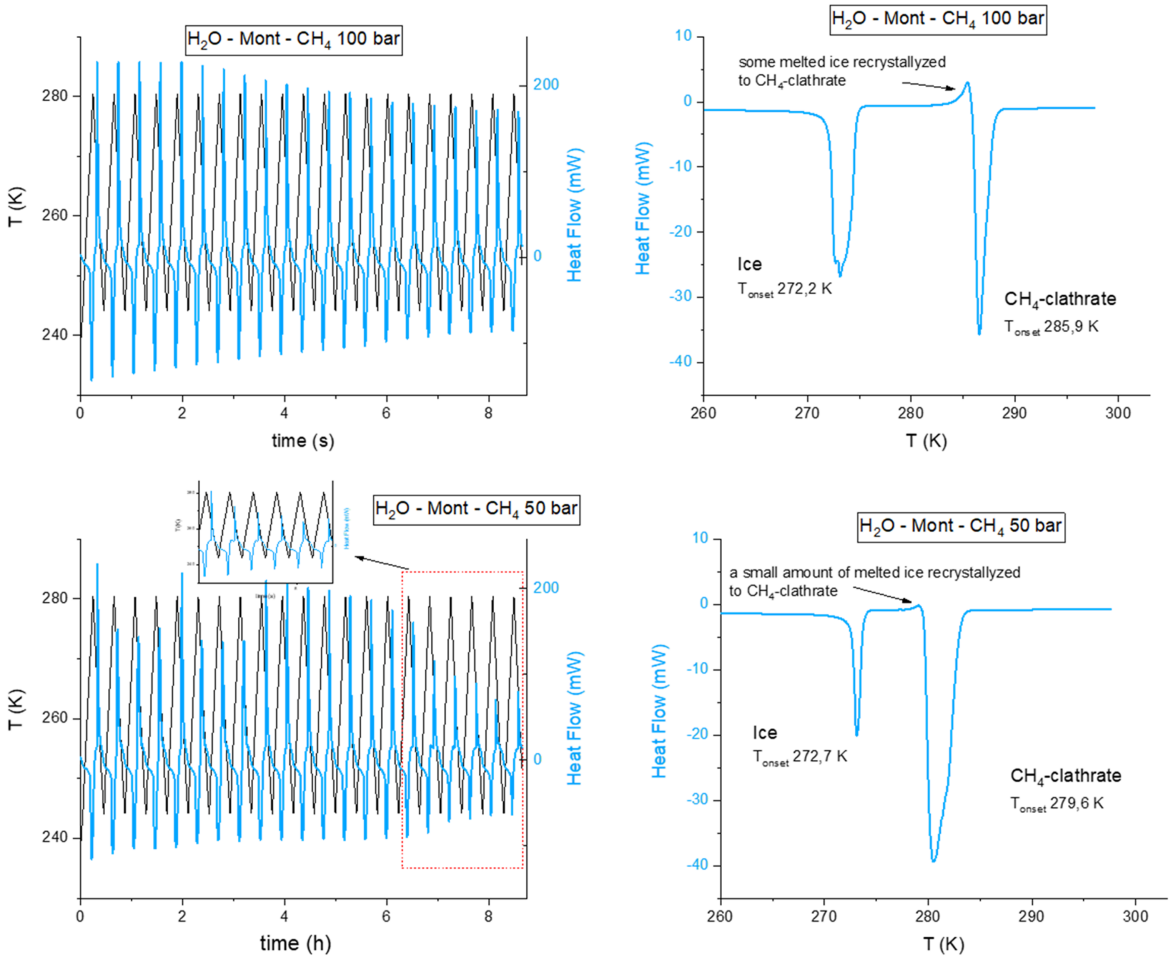

Figure A5. H_2O–Mt–CH_4 Run 1.

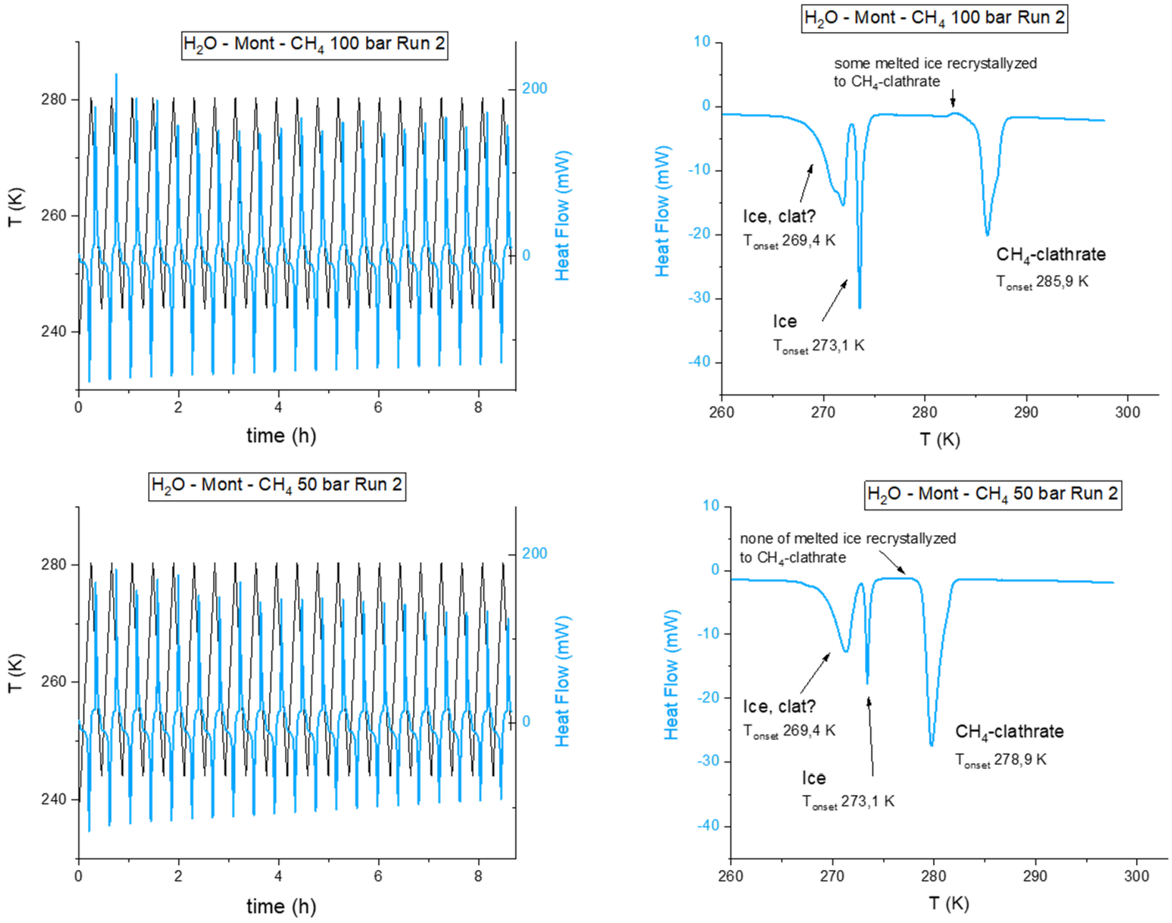

Figure A6. H_2O–Mt–CH_4 Run 2.

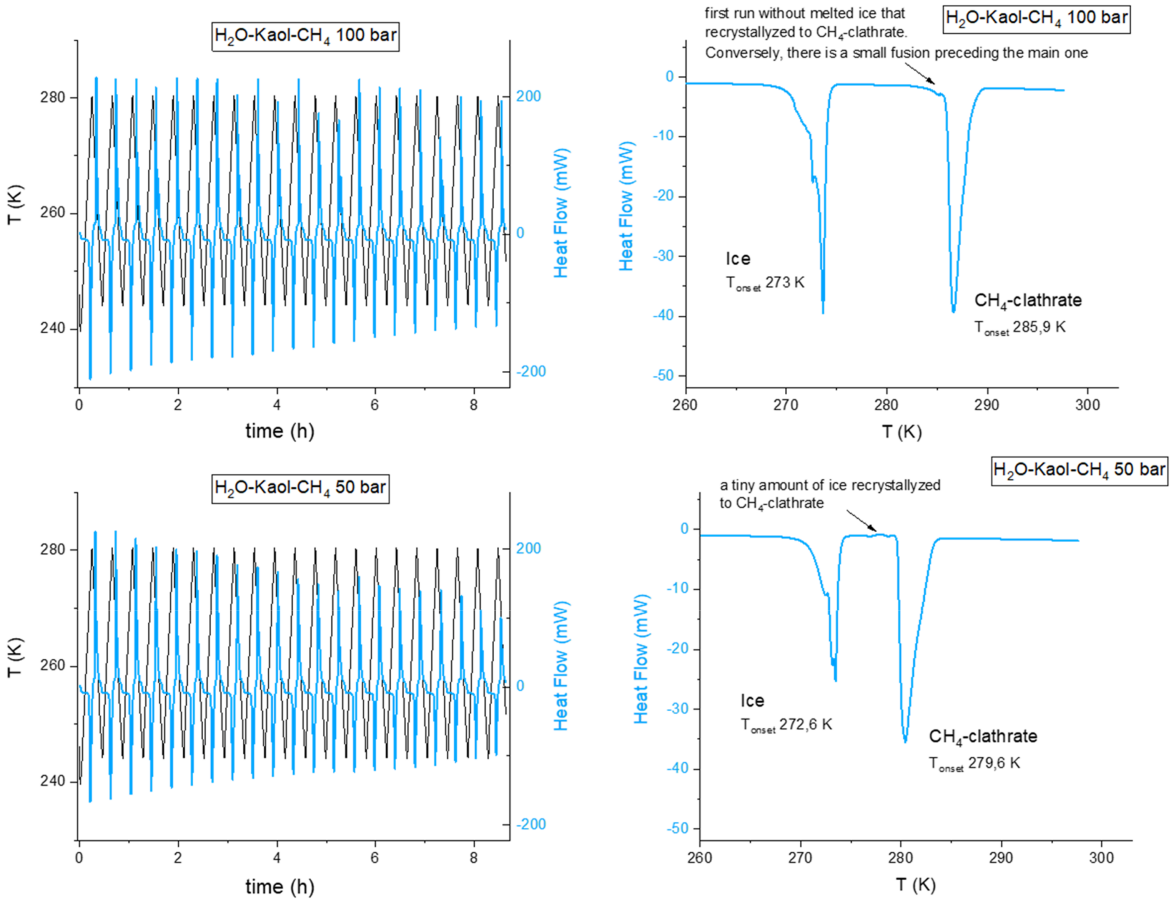

Figure A7. H_2O–Kaol–CH_4 Run 1.

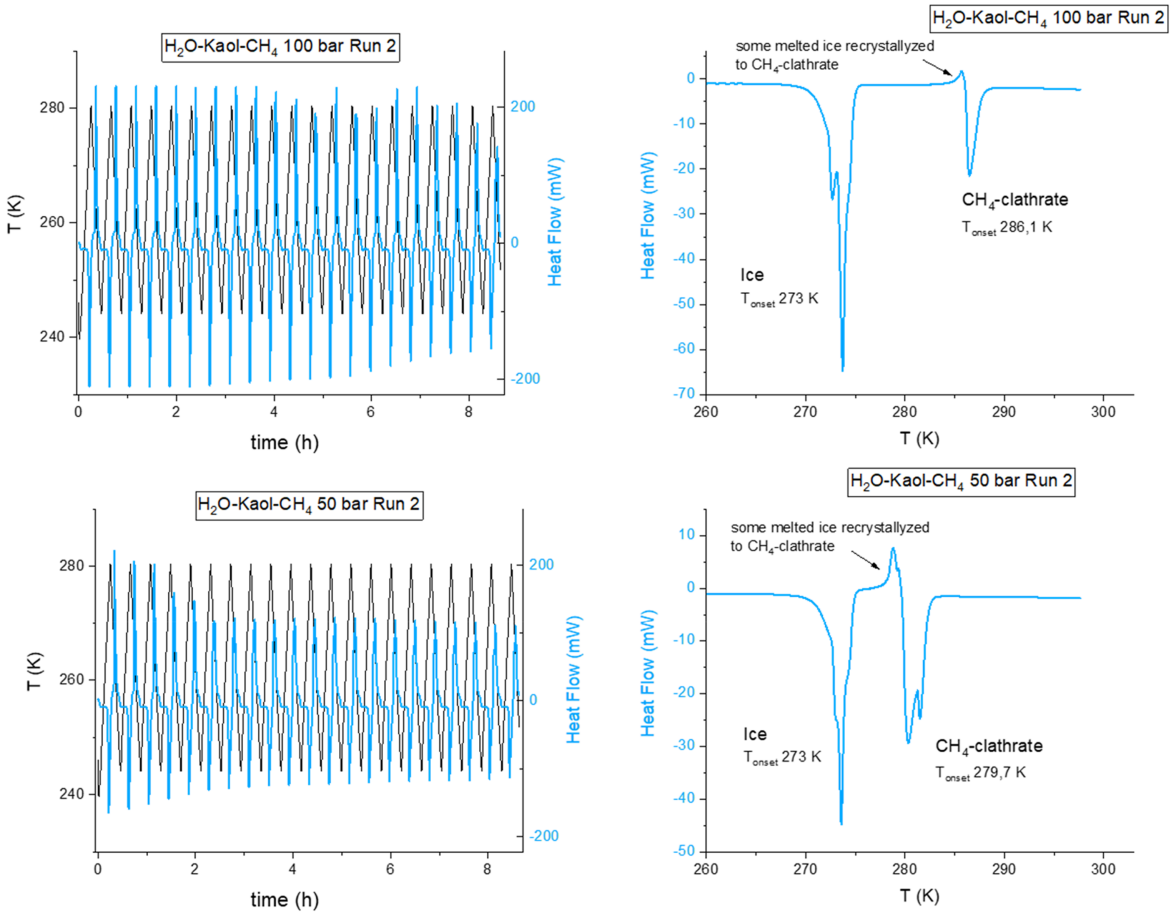

Figure A8. H_2O–Kaol–CH_4 Run 2.

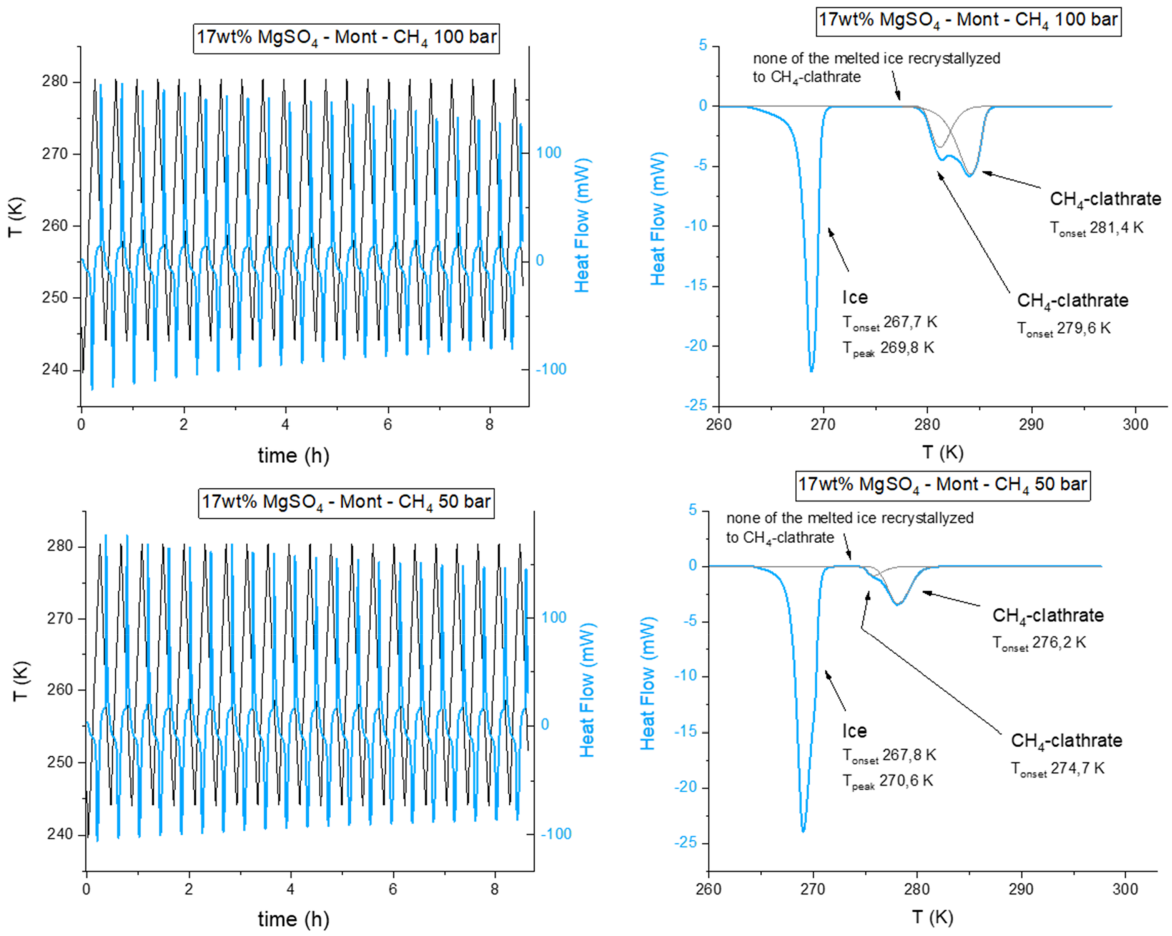

Figure A9. 17wt% $MgSO_4$–Mt–CH_4 Run 1.

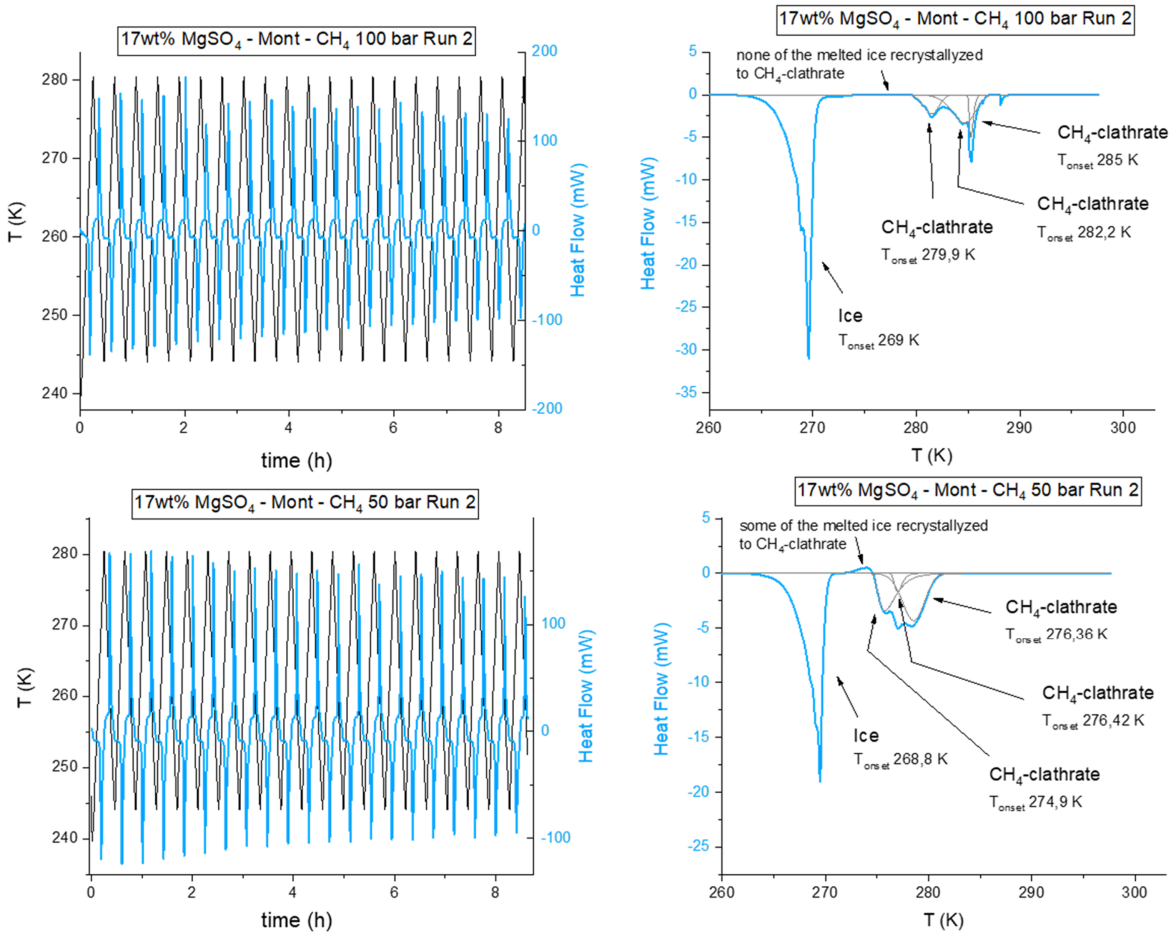

Figure A10. 17wt% $MgSO_4$–Mt–CH_4 Run 2.

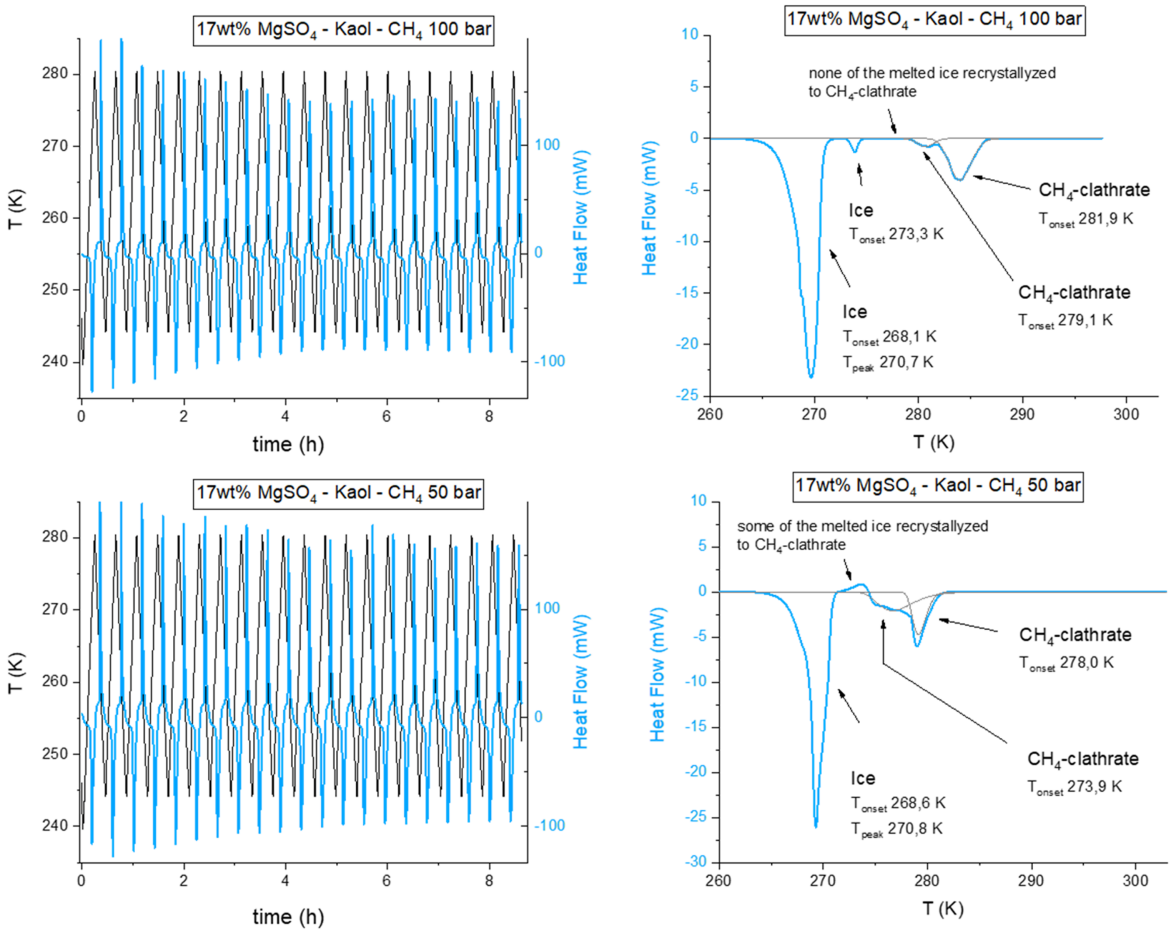

Figure A11. 17wt% $MgSO_4$–Kaol–CH_4 Run 1.

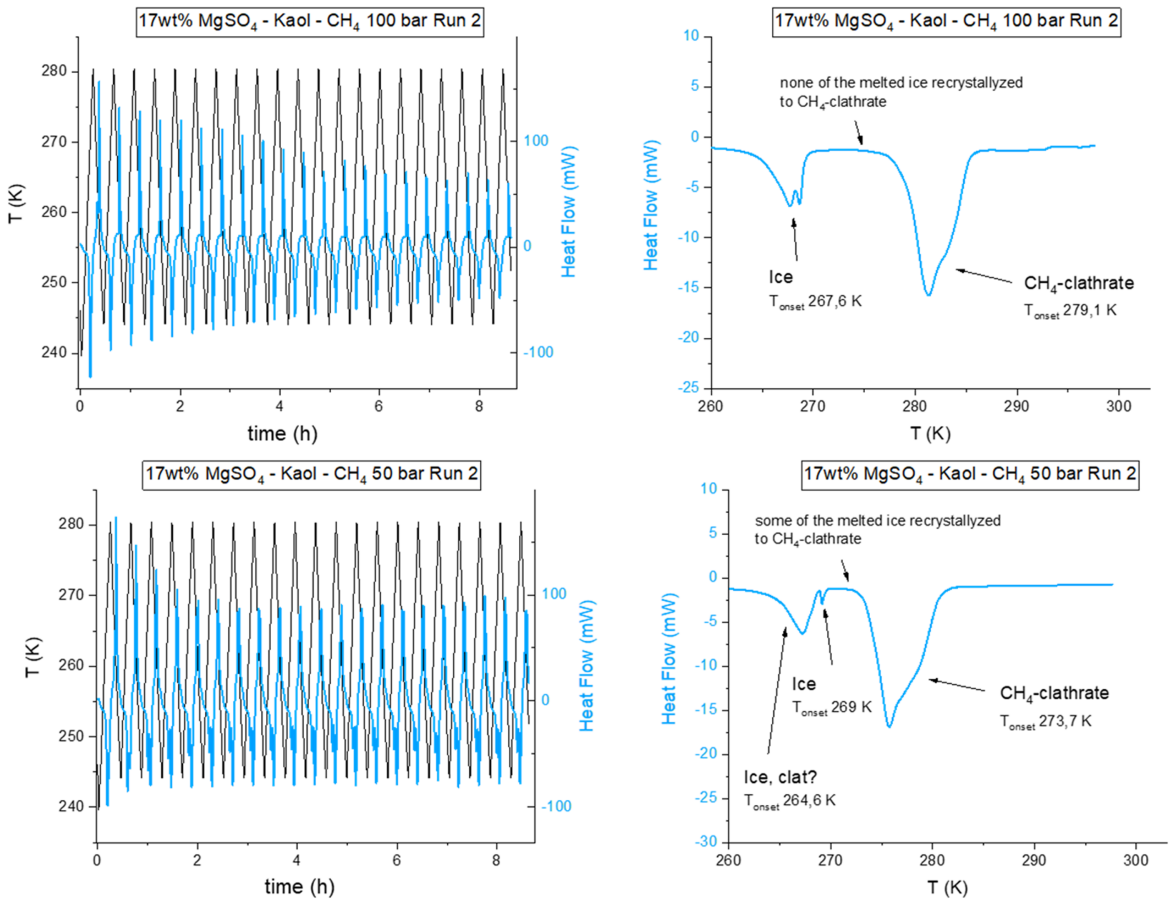

Figure A12. 17wt% $MgSO_4$–Kaol–CH_4 Run 2.

Appendix B

Table B1 shows the raw data obtained from the thermograms of each experiment and enthalpy (ΔH) and mass fraction (m) calculations.

Table B1
Raw Data Obtained from the Thermograms of Each Experiment

Systems	mt	Hi (exp)	His (theor)	mi	Hc (exp)	Hcs (exp)	mc	mw	Xi	Xc	Xw	Tdis Ice	Tdis Clat
Run 1	...	...	...	...	...	...	...	...	...	...	...	...	...
1.1. CH4-H2O, 100 bar	0,0815	11,4	333	0,0342	24,9	526,5	0,0473	0,0000	0,420	0,580	0,000	272,8	285,8
1.2. CH4-H2O, 50 bar	0,0815	15,449	333	0,0464	15,8	449,8	0,0351	0,0000	0,569	0,431	0,000	272,7	279,4
2.1. CH4-17wtMgSO4, 100 bar	0,0840	0,673	226	0,0030	26,7	526,5	0,0507	0,0304	0,035	0,603	0,361	269,1	281
2.2. CH4-17wtMgSO4, 50 bar	0,0840	3,77	226	0,0167	22,7	449,8	0,0505	0,0168	0,199	0,602	0,200	268,3	275.3
3.1. CH4-Mont-H2O, 100 bar	0,1260	15,053	333	0,0452	11,8	526,5	0,0224	0,0584	0,359	0,178	0,463	272,2	285,9
3.2. CH4-Mont-H2O, 50 bar	0,1260	4,669	333	0,0140	25,6	449,8	0,0570	0,0550	0,111	0,452	0,437	272,7	279,6
4.1. CH4-Kaol-H2O, 100 bar	0,1300	14,373	333	0,0432	17,4	526,5	0,0330	0,0538	0,332	0,254	0,414	273	285,9
4.2. CH4-Kaol-H2O, 50 bar	0,1300	9,952	333	0,0299	19,2	449,8	0,0427	0,0574	0,230	0,328	0,442	272,6	279,6
5.1. CH4-Mont-17wtMgSO4, peak 1, 100 bar	0,1370	10,837	226	0,0480	2,4	526,5	0,0046	0,0844	0,350	0,034	0,616	269,8	279,6
5.1. CH4-Mont-17wtMgSO4,peak 2, 100 bar	0,1370	10,837	226	0,0480	4,8	526,5	0,0091	0,0800	0,350	0,066	0,584	...	281,4
5.1. CH4-Mont-17wtMgSO4,peak 3, 100 bar	…	…	…	…	…	…	…	…	…	…	…	…	…
5.1. CH4-Mont-17wtMgSO4, total, 100 bar	0,1370	10,837	226	0,0480	7,2	526,5	0,0137	0,0753	0,350	0,100	0,550	...	...
5.2. CH4-Mont-17wtMgSO4, peak 1, 50 bar	0,1370	13,913	226	0,0616	0,5	449,8	0,0010	0,0744	0,449	0,008	0,543	270,6	274,7
5.2. CH4-Mont-17wtMgSO4, peak 2, 50 bar	0,1370	13,913	226	0,0616	2,6	449,8	0,0058	0,0696	0,449	0,043	0,508	...	273,2
5.2. CH4-Mont-17wtMgSO4, peak 3, 50 bar	…	…	…	…	…	…	…	0,0000	…	…	…	…	…
5.2. CH4-Mont-17wtMgSO4, total, 50 bar	0,1370	13,913	226	0,0616	3,1	449,8	0,0069	0,0686	0,449	0,050	0,500	…	…
6.1. CH4-Kaol-17wtMgSO4, peak 1, 100 bar	0,1330	15,817	226	0,0700	0,5	526,5	0,0009	0,0622	0,526	0,006	0,467	270,7	279,1
6.1. CH4-Kaol-17wtMgSO4, peak 2, 100 bar	0,1330	0,303	226	0,0013	3,2	526,5	0,0060	0,1256	0,010	0,045	0,945	273,3	281,9
6.1. CH4-Kaol-17wtMgSO4, total, 100 bar	0,1330	15,817	226	0,0700	3,6	526,5	0,0068	0,0562	0,526	0,051	0,422	...	...
6.2. CH4-Kaol-17wtMgSO4, peak 1, 50 bar	0,1330	13,96	226	0,0618	2,7	449,8	0,0059	0,0653	0,464	0,044	0,491	270,8	273,9
6.2. CH4-Kaol-17wtMgSO4, peak 2, 50 bar	0,1330	13,96	226	0,0618	2,3	449,8	0,0052	0,0660	0,464	0,039	0,497	...	278
6.2. CH4-Kaol-17wtMgSO4, total, 50 bar	0,1330	13,96	226	0,0618	4,7	449,8	0,0104	0,0608	0,464	0,078	0,457	...	...
Run 2	...	...	...	...	...	...	...	...	...	...	...	...	...
1.1. CH4-H2O, 100 bar	0,0784	5,79	333	0,0174	29,4	481,1	0,0610	0,0000	0,222	0,778	0,000	273,1	285,3
1.2. CH4-H2O, 50 bar	0,0784	0,929	333	0,0028	12,7	167,6	0,0756	0,0000	0,036	0,964	0,000	273,1	279,4
2.1. CH4-17wtMgSO4, 100 bar	0,0791	2,511	226	0,0111	20,5	481,1	0,0426	0,0254	0,140	0,538	0,321	269,2	281.5
2.2. CH4-17wtMgSO4, 50 bar	0,0791	0,472	226	0,0021	22,3	449,8	0,0497	0,0273	0,026	0,628	0,346	269,2	275.2
3.1. CH4-Mont-H2O, 100 bar	0,1260	15,137	333	0,0455	8,1	481,1	0,0169	0,0636	0,361	0,134	0,505	269,4	285,9
3.2. CH4-Mont-H2O, 50 bar	0,1260	9,83	333	0,0295	12,1	449,8	0,0269	0,0696	0,234	0,214	0,552	269,4	278,9
4.1. CH4-Kaol-H2O, 100 bar	0,1380	25,569	333	0,0768	6,0	481,1	0,0125	0,0487	0,556	0,091	0,353	273	286,1
4.2. CH4-Kaol-H2O, 50 bar	0,1380	18,079	333	0,0543	15,0	449,8	0,0333	0,0505	0,393	0,241	0,366	273	279,7
5.1. CH4-Mont-17wtMgSO4,peak 1, 100 bar	0,1280	13,649	226	0,0604	1,2	481,1	0,0026	0,0650	0,472	0,020	0,508	269	279,9
5.1. CH4-Mont-17wtMgSO4, peak 2, 100 bar	0,1280	13,649	226	0,0604	2,8	481,1	0,0058	0,0618	0,472	0,046	0,483	…	282,2
5.1. CH4-Mont-17wtMgSO4, peak 3, 100 bar	0,1280	13,649	226	0,0604	0,7	481,1	0,0016	0,0660	0,472	0,012	0,516	…	285
5.1. CH4-Mont-17wtMgSO4, total, 100 bar	0,1280	13,649	226	0,0604	4,8	481,1	0,0099	0,0577	0,472	0,078	0,451	…	…
5.2. CH4-Mont-17wtMgSO4, peak 1, 50 bar	0,1280	9,384	226	0,0415	2,3	449,8	0,0051	0,0814	0,324	0,040	0,636	268,8	274,9
5.2. CH4-Mont-17wtMgSO4, peak 2, 50 bar	0,1280	9,384	226	0,0415	0,5	449,8	0,0010	0,0854	0,324	0,008	0,668	…	276,42
5.2. CH4-Mont-17wtMgSO4, peak 3, 50 bar	0,1280	9,384	226	0,0415	3,4	449,8	0,0077	0,0788	0,324	0,060	0,616	…	276,36
5.2. CH4-Mont-17wtMgSO4, total, 50 bar	0,1280	9,384	226	0,0415	6,2	449,8	0,0137	0,0727	0,324	0,107	0,568	…	…
6.1. CH4-Kaol-17wtMgSO4, peak 1, 100 bar	0,1315	5,231	226	0,0231	17,7	481,1	0,0368	0,0715	0,176	0,280	0,544	267,6	279,1
6.1. CH4-Kaol-17wtMgSO4, peak 2, 100 bar	…	…	…	…	…	…	…	…	…	…	…	…	…
6.1. CH4-Kaol-17wtMgSO4, total, 100 bar	…	…	…	…	…	…	…	…	…	…	…	…	…
6.2. CH4-Kaol-17wtMgSO4, peak 1, 50 bar	0,1315	3,851	226	0,0170	20,2	449,8	0,0448	0,0696	0,130	0,341	0,530	264,6	273,7

Table B1
(Continued)

Systems	mt	Hi (exp)	His (theor)	mi	Hc (exp)	Hcs (exp)	mc	mw	Xi	Xc	Xw	Tdis Ice	Tdis Clat
6.2. CH4-Kaol-17wtMgSO4, peak 2, 50 bar	0,1315	0,147	226	0,0007	…	449,8	0,0000	0,1308	…	…	…	269	…
6.2. CH4-Kaol-17wtMgSO4, total, 50 bar	…	…	…	…	…	…	…	…	…	…	…	…	…

Note. The table shows the enthalpy values without mass normalization of ice (Hi) and clathrate (Hc), the mass and fraction of ice (mi, Xi), clathrate (mc, Xc), and residual water (mw, Xw) formed upon cooling, the specific enthalpies of dissociation (after mass correction) of ice (His) and clathrate (Hcs), and the dissociation temperatures of ice and clathrate (Tdis ice, Tdis clat).

ORCID iDs

Victoria Muñoz-Iglesias https://orcid.org/0000-0002-1159-9093
Elodie Gloesener https://orcid.org/0009-0001-8340-3192
Carolina Gil-Lozano https://orcid.org/0000-0003-3500-2850
Mathieu Choukroun https://orcid.org/0000-0001-7447-9139
Olga Prieto-Ballesteros https://orcid.org/0000-0002-2278-1210
Maite Fernández Sampedro https://orcid.org/0000-0003-1932-7591
Valentín García Baonza https://orcid.org/0000-0001-9994-0980
Gabriel Tobie https://orcid.org/0000-0002-4494-0294

References

Achilles, C. N., Rampe, E. B., Downs, R. T., et al. 2020, JGRE, 125, e2019JE006295
Atreya, S. K., Mahaffy, P. R., & Wong, A.-S. 2007, P&SS, 55, 358
Bian, H., Ai, L., Hellgardt, K., Maitland, G. C., & Heng, J. Y. Y. 2021, Cryst, 11, 201
Botan, A., Rotenberg, B., Marry, V., Turq, P., & Noetinger, B. 2010, J. Phys. Chem. C, 114, 14962
Bristow, T. F., Rampe, E. B., Achilles, C. N., et al. 2018, SciA, 4, eaar3330
Cai, W., Huang, X., & Lu, H. 2022, Energ, 15, 485
Castellini, E., Malferrari, D., Bernini, F., et al. 2017, CCM, 65, 220
Chastain, B. K., & Chevrier, V. 2007, P&SS, 55, 1246
Chevrier, V., & Mathé, P. E. 2007, P&SS, 55, 289
Emmerich, K., Wolters, F., Kahr, G., et al. 2009, CCM, 57, 104
Farrell, W. M., Delory, G. T., & Atreya, S. K. 2006, GeoRL, 33, L21203
Formisano, V., Atreya, S., Encrenaz, T., Ignatiev, N., & Giuranna, M. 2004, Sci, 306, 1758
Geyer, C., Elwood Madden, A. S., Rodriguez, A., et al. 2023, PSJ, 4, 48
Gil-Lozano, C., Fairén, A. G., Muñoz-Iglesias, V., et al. 2020, NatSR, 10, 15097
Gloesener, E., Karatekin, Ö., & Dehant, V. 2021, Icar, 353, 114099
González Sánchez, F., Jurányi, F., Gimmi, T., et al. 2008, JPCM, 20, 415102
Gough, R. V., Tolbert, M. A., McKay, C. P., & Toon, O. B. 2010, Icar, 207, 165
Grant, J. A., Wilson, S. A., Mangold, N., Calef, F., & Grotzinger, J. P. 2014, GeoRL, 41, 1142
Grotzinger, J. P., Gupta, S., Malin, M. C., et al. 2015, Sci, 350, aac7575
Jones, E. G., Lineweaver, C. H., & Clarke, J. D. 2011, AsBio, 11, 1017
Kim, D., Ahn, Y.-H., Kim, S.-J., et al. 2015, J. Phys. Chem. C, 119, 22148
Knak Jensen, S. J., Skibsted, J., Jakobsen, H. J., et al. 2014, Icar, 236, 24
Knutsen, E. W., Villanueva, G. L., Liuzzi, G., et al. 2021, Icar, 357, 114266
Korablev, O., Vandaele, A. C., Montmessin, F., et al. 2019, Natur, 568, 517
Kozlowski, T. 2011, Cold Reg. Sci. Technol., 68, 139
Krasnopolsky, V. A., Maillard, J. P., & Owen, T. C. 2004, Icar, 172, 537
Lafond, P. G., Grim, R. G., & Sum, A. K. 2015, Can. J. Chem., 93, 826
Lamorena, R. B., & Lee, W. 2008, EnST, 42, 2753
Lefèvre, F., & Forget, F. 2009, Natur, 460, 720
Li, Y., Chen, M., Liu, C., et al. 2020a, Langm, 36, 3323
Li, Y., Chen, M., Song, H., et al. 2020b, Appl. Clay Sci., 186, 105439
Li, Y., Wu, N., He, C., et al. 2021, Fuel, 291, 120103
Li, Y., Han, S., Zhang, B., et al. 2022, Appl. Clay Sci., 216, 106344
Lin, W., Dalmazzone, D., Fürst, W., et al. 2013, J. Chem. Thermodyn., 61, 132
Longhi, J. 2006, J. Geophys. Res., 111, 2005JE002552
Martos-Villa, R., Guggenheim, S., Mata, M. P., Sainz-Diaz, C. I., & Nieto, F. 2014, Am. Mineral., 99, 401
Max, M., Johnson, A., & Clifford, S. 2011, in Proceedings of the 7th International Conference on Gas Hydrates (ICGH 2011) (Curran Associates, Inc.)
Méndez, A. S. J., Muñoz-Iglesias, V., Izquierdo-Ruíz, F., & Prieto-Ballesteros, O. 2017, J. Phys.: Conf. Ser., 950, 042042
Montmessin, F., Korablev, O. I., Trokhimovskiy, A., et al. 2021, A&A, 650, A140
Moores, J. E., Gough, R. V., Martinez, G. M., et al. 2019a, Nat. Geosci., 12, 321
Moores, J. E., King, P. L., Smith, C. L., et al. 2019b, GeoRL, 46, 9430
Mumma, M. J., Villanueva, G. L., Novak, R. E., et al. 2009, Sci, 323, 1041
Muñoz-Iglesias, V., & Prieto-Ballesteros, O. 2021, ACS Earth Space Chem, 5, 2626
Muñoz-Iglesias, V., Fernandez-Sampedro, M., Gil-Lozano, C., et al. 2021, Appl. Clay Sci., 209, 106137
Muñoz-Iglesias, V., Prieto-Ballesteros, O., & López, I. 2019, JGRE, 124, 2660
Nakamura, R., & Ohtani, E. 2011, Icar, 211, 648
Oehler, D. Z., & Etiope, G. 2017, AsBio, 17, 1233
Oze, C., & Sharma, M. 2005, GeoRL, 32, L10203
Palucis, M. C., Dietrich, W. E., Hayes, A. G., et al. 2014, JGRE, 119, 705
Park, S.-H., & Sposito, G. 2003, J. Phys. Chem. B, 107, 2281
Park, T., Kyung, D., & Lee, W. 2014, EnST, 48, 6597
Petuya, C., Choukroun, M., Vu, T., et al. 2020, Chem. Commun., 56, 12391
Pla-Garcia, J., Rafkin, S. C. R., Karatekin, Ö., & Gloesener, E. 2019, JGRE, 124, 2141
Prieto-Ballesteros, O., Kargel, J. S., Fernández-Sampedro, M., et al. 2005, Icar, 177, 491
Prieto-Ballesteros, O., Kargel, J. S., Fairén, A. G., et al. 2006, Geo, 34, 149
Prieto-Ballesteros, O., Muñoz-Iglesias, V., & Bonales, L. J. 2022, MNRAS, 515, 3512
Rapin, W., Ehlmann, B. L., Dromart, G., et al. 2019, Nat. Geosci., 12, 889
Ren, J., Zeng, S., Chen, D., et al. 2023, Appl. Energy, 340, 120997
Robustillo, M. D., Menezes, D. E. S. de, & Pessôa Filho, P. de A. 2022, Fuel, 312, 122896
Root, M. J., & Elwood Madden, M. E. 2012, Icar, 218, 534
Safi, E., Thompson, S. P., Evans, A., et al. 2017, A&A, 600, A88
Safi, E., Thompson, S. P., Evans, A., et al. 2019, GeCoA, 245, 304
Sloan, E. D., & Koh, C. A. 2008, Clathrate Hydrates of Natural Gases (3rd ed.; CRC Press)
Suarez, D. L., & Zahow, M. F. 1989, SSASJ, 53, 52
Sun, L. 2016, PhD thesis, Univ. Eastern Finland
Sun, R., Fan, Z., Yang, L., et al. 2020, Chin. J. Chem. Eng., 28, 949
Sun, Y., Jiang, S., Li, S., Wang, X., & Peng, S. 2021, Chem. Eng. J., 406, 126872
Tamamura, S., Takada, T., Tomita, J., et al. 2014, J. Radioanal. Nucl. Chem., 299, 569
Tao, Y., Yan, K., Li, X., et al. 2020, Energ, 13, 231
Thomas, C., Mousis, O., Picaud, S., & Ballenegger, V. 2009, P&SS, 57, 42
Thomson, B. J., Bridges, N. T., Milliken, R., et al. 2011, Icar, 214, 413
Thorpe, M. T., Bristow, T. F., Rampe, E. B., et al. 2022, JGRE, 127, e2021JE007099
Trainer, M. G., Tolbert, M. A., McKay, C. P., & Toon, O. B. 2010, Icar, 208, 192
Toner, J. D., Catling, D. C., & Light, B. 2014, Icar, 233, 36
Tu, V. M., Rampe, E. B., Bristow, T. F., et al. 2021, Mine, 11, 847
Villanueva, G. L., Mumma, M. J., Novak, R. E., et al. 2013, Icar, 223, 11
Wang, R., Liao, B., Wang, J., Sun, J., et al. 2023, Chem. Eng. J., 451, 138757
Wang, X., Yuan, Y., Du, Z., et al. 2025, Pet. Sci., 22, 3029
Webster, C. R., Mahaffy, P. R., Atreya, S. K., et al. 2015, Sci, 347, 415
Webster, C. R., Mahaffy, P. R., Atreya, S. K., et al. 2018, Sci, 360, 1093
Webster, C. R., Mahaffy, P. R., Pla-Garcia, J., et al. 2021, A&A, 650, A166
Wei, Y., & Maeda, N. 2023, Chem. Eng. Sci., 270, 118538
Weiss, B. P., Yung, Y. L., & Nealson, K. H. 2000, PNAS, 97, 1395
White, G. N. 1992, Clays Clay Miner, 40, 555
Yan, K., Li, X., Chen, Z., et al. 2019, Chin. J. Chem. Eng., 27, 1212
Yesilbaş, M. 2018, PhD Thesis, Umeå Univ.
Yesilbaş, M., Lee, C. C., & Boily, J.-F. 2018, ESC, 2, 314
Zahnle, K. 2015, Sci, 347, 370
Zahnle, K., Freedman, R. S., & Catling, D. C. 2011, Icar, 212, 493
Zhang, X., Berkinsky, D., Markus, C. R., et al. 2022, Icar, 376, 114832